





Review

Butane Isomerization as a Diagnostic Tool in the Rational Design of Solid Acid Catalysts

Matthew E. Potter ^{1,*} , Joshua J.M. Le Brocq ¹ , Alice E. Oakley ¹ , Evangeline B. McShane ¹,
Bart D. Vandegehuchte ² and Robert Raja ^{1,*} 

¹ Chemistry Department, University of Southampton, Southampton, Hants SO17 1BJ, UK;

j.jlb1g14@soton.ac.uk (J.J.M.L.B.); A.E.Oakley@soton.ac.uk (A.E.O.); E.B.McShane@soton.ac.uk (E.B.M.)

² Total Research & Technology Feluy, Zone Industrielle Feluy C, B-7181 Seneffe, Belgium;
bart.vandegehuchte@total.com

* Correspondence: M.E.Potter@soton.ac.uk (M.E.P.); R.Raja@soton.ac.uk (R.R.)

Received: 13 August 2020; Accepted: 18 September 2020; Published: 22 September 2020



Abstract: The growing demand for isobutane as a vital petrochemical feedstock and chemical intermediate has for many decades surpassed industrial outputs that can be supplied through liquified petroleum gases. Alternative methods to resource the isobutane market have been explored, primarily the isomerization of linear *n*-butane to the substituted isobutane. To date the isobutane market is valued at over 20 billion US dollars, enticing researchers to seek unique and novel catalytic materials to improve on current commercial practices. Two main classes of catalysts have dominated the butane isomerization literature in the last few decades; namely microporous zeolites and sulfated zirconia. Both have been widely researched for butane isomerization, to the point where key catalytic descriptors such as acidity, framework topology and metal doping are becoming well understood. While this provides new researchers with a roadmap for developing new materials, it has also begun developing into an invaluable tool for diagnosing and understanding the effect of these individual descriptors on catalytic properties. In this review we explore the different factors that influence the active site behavior of particularly zeolites and sulfated zirconia catalysts towards understanding the use of butane isomerization as a diagnostic tool for solid-acid catalysts.

Keywords: zeolites; butane isomerization; sulfated zirconia; acidity; solid-acid catalysts

1. Commercial and Fundamental Aspects of Butane Isomerization

Liquified petroleum gas (LPG) is a vital and growing industry, used globally as household fuels, motor fuel additives and as a replacement refrigerant for CFCs. Typically, 60% of LPG is recovered from natural gas extraction from the earth, whereas the remaining 40% is produced from crude oil refining [1]. To date roughly 320 million metric tons of LPG are produced around the world, which consistently increases year on year by around an extra 10 million metric tons per year [2]. This is primarily due to the growing supplies from North America, Asia and the Middle East [2]. The precise content of LPG varies regionally, with differing proportions of butane isomers and propane, [3] though in 2014 it was estimated that *n*-butane and isobutane accounted for 19% of all hydrocarbon gas liquids in the US [4]. The butane market is also predicted to steadily grow over the next decade. Its value was estimated as \$60.0 billion in 2015 [5,6], with recent reports estimating this will grow to \$81.6 billion by 2025 [6]. One of the key reasons for this increase is the demand for isobutane, which while valued at \$20 billion in 2018, is estimated to reach \$34 billion by 2026 [7]. Between 2008 and 2014, isobutane production in the US increased by 43%, that was linked to the shale gas boom during that time [4]. The demand for isobutane, specifically, is attributed to its role as a valuable feedstock for high octane fuels (alkylates) [8–10], chemical intermediates (Figure 1) [11], and its growing use as a propellant and calibrant [7]. Typically,

gasoline is blended with between 2–3% of butanes, however reports have suggested that this can viably increase to 10%, in certain conditions [12]. Though the demand for isobutane has been tied to the demand and pricing of alkylates [13]. In the 1930s it was realized that demand for isobutane would surpass the supply from natural gas and refining alone, leading to the development of processes to isomerize *n*-butane to isobutane [11]. This process has since evolved, to the point that the largest US butane plant (as of 2015) in Mont Belvieu, Texas creates 116 MBPD of isobutane through butane isomerization [14].

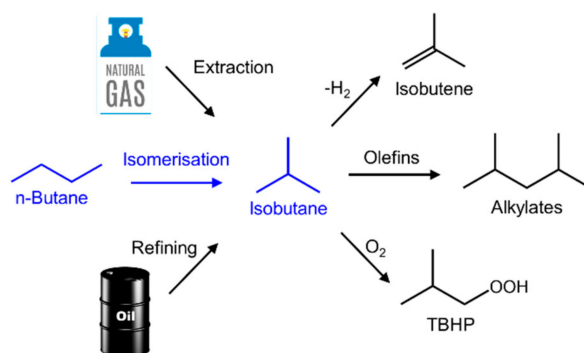


Figure 1. Main production pathways and uses for isobutane.

Some of the earliest works on butane isomerization used a combination of HCl and aluminum chloride catalyst [10]. Industrial implementation of this technology was hampered due to the aluminum chloride subliming, and then solidifying to block the flow [15]. Further the high temperatures caused the aluminum source to become sparingly soluble in the hydrocarbon flow, causing a significant loss of the catalyst. In 1941 UOP circumvented these issues with a Pt-modified, chlorinated alumina catalyst (Pt/Al₂O₃-Cl) with the Butamer process [15]. The UOP Butamer process remains the main butane isomerization process to date, though unsurprisingly the technology has undergone several iterations since its creation [10]. Currently there are over 85 Butamer plants operating worldwide, making it the primary butane isomerization process [16]. To date a range of commercial processes exist, typically focussing on either chlorinated alumina or sulfated zirconia catalysts (Table 1) [17–20].

Table 1. Comparing commercial butane isomerization processes. Adapted from [19] and [21–23].

Process	Butamer	C ₄ Isom	BIC	CFB-Isom	Lummus	Isomalk-3
Company	UOP	BP	Boreskov Institute of Catalysis	UPC	Lummus	JSC SIE Neftheim
Catalyst	Pt/Al ₂ O ₃ -Cl	Pt/Al ₂ O ₃ -Cl	Pd/SO ₄ .ZrO ₂	SO ₄ /ZrO ₂ .Al ₂ O ₃	Al ₂ O ₃ -Cl	Pt/SO ₄ .ZrO ₂
Pressure/Bar	25–32	14–28	23–25	1–1.5	4–10	>15
Temperature/°C	160–220	150–200	120–160	160–200	100–160	180–200
Feed additives	Chlorides	Chlorides	None	None	Chlorides	None
Butane/H ₂ mol ratio	14–34	Unknown	7–20	No H ₂	Unknown	10–17
Minimum conversion/mol%	50	Unknown	60	52	60	50
Minimum selectivity/mol%	98	95	90	72	99	90
Caustic output	Yes	Yes	No	No	Yes	No

This list is by no means exhaustive, with the pool of companies developing their own isomerization catalysts constantly increasing, including Axens (ATIS-1L), Shell (Hysomer) and Clariant (Hysopar 6000) [8]. Note that most commercial processes operate below 220 °C, this is due to butane isomerization being slightly exothermic [24]. Thus, conversions are capped by the chemical equilibrium (Figure 2), creating a compromise between isobutane yield, and production rate.

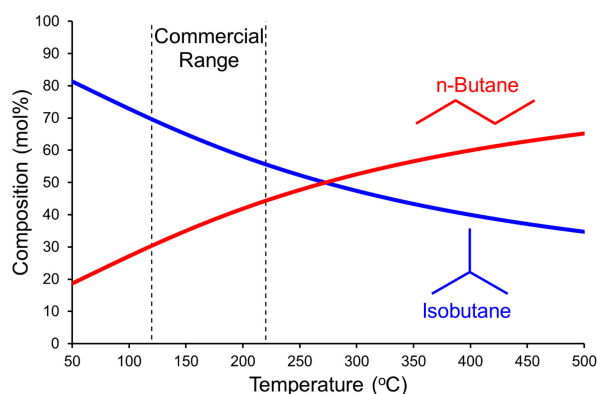


Figure 2. Chemical equilibrium for butane/isobutane gas mixtures, using data from [24].

The kinetics of the isomerization process is heavily dependent on which reaction mechanism occurs [5,25]. Presently there are two identified mechanisms, denoted as monomolecular and bimolecular pathways. The monomolecular pathway is initiated by protonation of *n*-butane, by Brønsted acid sites (BAS), leading to a secondary carbonium ion, which undergoes dehydrogenation to yield a secondary carbenium ion [26–29]. In some cases, these positively charged intermediates can be stabilized by oxygen atoms in the framework, yielding alkoxide species [30]. Initially it was believed that this carbenium ion then formed a methyl-cyclopropane intermediate, as observed in pentane and hexane isomerization. However, it has since been shown that such a species is actually a transition state, that leads to carbon scrambling, and not isobutane [19,31]. Instead a methyl shift may occur, resulting in a tertiary isobutyl carbenium ion (Figure 3). The carbenium intermediates are then neutralized by hydrogen transfer from other species, to form neutral products. These computational findings showed excellent agreement with experimental values, confirming this mechanism [19,31].

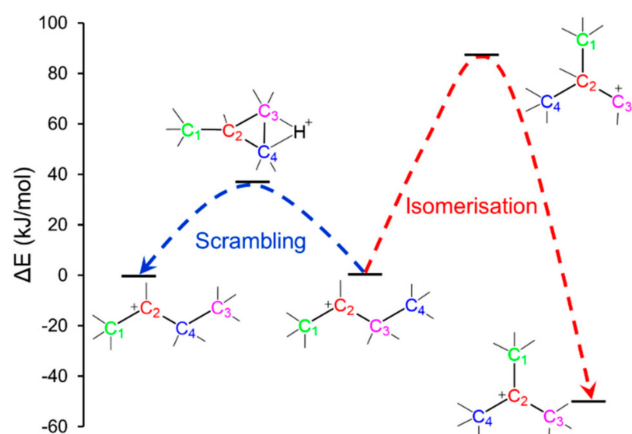


Figure 3. Theoretical findings based on the monomolecular isomerization pathway. Figure adapted from data in [19,31].

An alternative pathway, the bimolecular mechanism, hypothesizes the formation of $C_8H_{17}^+$ intermediate species, formed by the combination of the *n*-butyl carbenium with either a C_4 olefin, or another butane molecule, after dehydrogenation (Figure 4) [26–29]. The C_4 olefins are typically present as feed impurities, as separating butanes and butenes is incredibly challenging, or the olefins may be formed in the reaction by dehydrogenation of butane. The need to form butene in situ for this pathway, is one of the reasons why many industrial catalysts (Table 1) are bifunctional, containing both acidic and noble metal species [20]. Once formed these C_8 intermediates can undergo either even scission, leading to isomerization, or uneven scission leading to disproportionation.

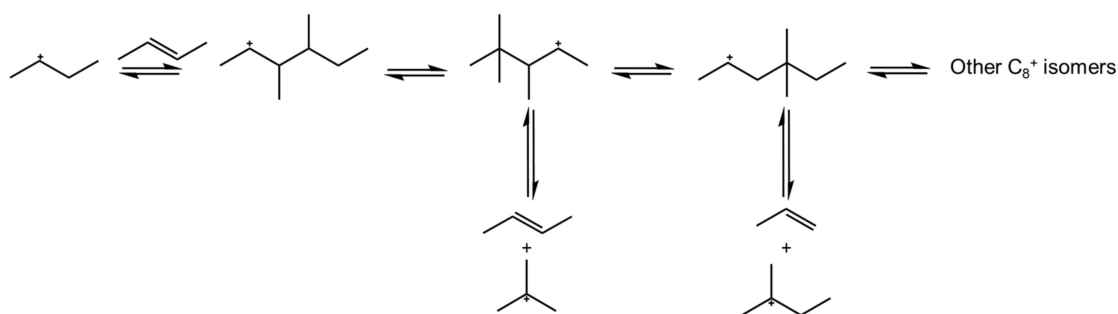


Figure 4. Summary of the bimolecular pathway mechanism with possible products.

Under these conditions olefins and alkanes can rapidly interchange, with metal sites and hydrogen feedstocks promoting hydrogenation and dehydrogenation during the reaction, leading to a wide array of possible alkane and olefin products. The precise mechanism followed depends on the conversion achieved, temperatures and pressures used, as well as the catalyst itself. The monomolecular pathway requires strongly acidic catalysts, with high temperatures and lower butane partial pressures. While the monomolecular pathway is more selective to isobutane, the stronger conditions required (typically > 300 °C), limit the maximum possible isobutane yield (Figure 2). In contrast the bimolecular mechanism operates at significant lower temperatures (<250 °C), lowering the energy input required. However, this process requires high partial pressures of butane, to maximize the chances of intermolecular collisions, leading to the formation of the C₈ intermediate [20]. The bimolecular pathway is also heavily based on hydrogen transfer, which is enhanced by a bifunctional catalyst. Further the density, not just the total quantity, of acid sites is known to play a key role in the kinetics of this reaction. It is also possible, in principle to control the pathway by modifying the space around active sites. A range of microporous species could not accommodate a C₈ intermediate, meaning that the monomolecular pathway would be preferred. Similarly, the precise framework topology could also be used to favor different C₈ species, leading to control over the scission pathways, selectively forming specific products (isobutane).

There exists a wealth of knowledge describing the mechanistic aspects of butane isomerization, best summarized in the reviews by Caeiro et al. and Y. Ono, who discuss this at great length [32,33]. Owing to this sensitivity to a wide range of catalytic descriptors, butane isomerization is recognized as a model reaction for the benchmarking and optimization of novel solid-acid catalysts [34]. Unlike these works, we discuss what effect individual catalytic descriptors have on reaction behavior, and how researchers may interpret and use these results as a means to characterize solid-acid materials. In particular, we will discuss the influence of framework topology, acid site location, strength and the role of metal dopants for a range of nanoporous species, as well as the influence of mesoporosity. Thanks to the in-depth understanding afforded from the mechanistic studies of butane isomerization in these prior works, *n*-butane isomerization represents a diagnostic tool for understanding solid-acid catalyst characteristics, leading to the development of generalized structure-property relationships for a range of acidic materials [34].

2. Tailoring Microporous Species for Butane Isomerization

2.1. Main Principles

Microporous zeolites and sulfated zirconias (SZs) [17,20] are two main groups of butane isomerization catalysts which have received extensive attention in the literature. However, generalized structure property correlations can be made and applied to a wide range of other solid acid catalysts, based on the intrinsic properties of these materials. This range includes Pt-doped chlorinated aluminas [35], aluminophosphates [36], heteropolyacids [37], silicas [38], molybdena [39], metal-doped zirconias [40] and ionic liquids [41], which are considerably less studied. An important distinction in

this review has been made between nanoporous zeolite systems and large pore catalysts, which includes both Zeolites and SZs.

Zeolites are primarily formed from SiO_4 tetrahedral units, joined through corner-sharing Si–O–Si bonds. In doing so they form different secondary building units, which can link in a range of ways to create different framework motifs. The precise framework which forms is determined by the synthesis conditions and reagents. The interest in zeolites derives from the ability to isomorphously substitute framework Si^{4+} sites with Al^{3+} , creating a “net negative charge”. This negative charge is then neutralized by a proton, associated with the framework, creating a BAS, hence their use as solid-acid catalysts [42]. This leads to protonated zeolites having the formula: $\text{H}_x\text{Al}_x\text{Si}_{1-x}\text{O}_2 \cdot y\text{H}_2\text{O}$. Similarly, it is also possible to form Lewis acid sites (LAS) in zeolites, where most commonly these are due to “extra-framework” aluminum species, which are not substituted directly into the framework. The wide range of possible zeolite topologies makes them excellent candidates for any reaction involving smaller hydrocarbon substrates, such as the isomerization of *n*-butane to isobutane. This is because the acid sites typically lie within the internal channels and cages of the nanoporous framework. This means, in principle, one can guide a reaction to a specific pathway by either hindering the formation of a bulky intermediate or trap larger products near the active site, forcing them to react further. These two approaches are known as “transition-state” and “product” selectivity (respectively) and form a key part of zeolite catalysis [43].

Aside from the choice of framework, it is also possible to control the acidic properties of a zeolite. Varying the quantity of aluminum incorporated into the same framework (the Si/Al ratio) influences the quantity of acid sites, the acid site strength, and the hydrophilicity of the system. From the zeolite formula above ($\text{H}_x\text{Al}_x\text{Si}_{1-x}\text{O}_2 \cdot y\text{H}_2\text{O}$), there is a 1:1 relationship between the protons and the substituted aluminum. Thus, zeolites with more framework substituted aluminum will have a greater number of acidic catalytic sites. However, this is limited as there cannot be more aluminum molecules than silicon in a zeolite, as this would result in “net negative charges”, from the Al^{3+} , being adjacent. This is prohibited by a phenomenon known as Lowenstein’s rule. It is also important to consider that while it is possible to increase the total number of acid sites in a zeolite, it does not mean that all the sites will be the same. A significant body of work shows that the Si/Al ratio is a key factor for determining acid strength, with not all frameworks behaving in the same manner. It has been shown that a lower Al content (higher Si/Al) ratio leads to stronger acid sites in faujasite (FAU) [44,45] and zeolite beta (BEA) [45,46], though weaker acid sites in ferrierite (FER) [45] and ZSM-5 (MFI) [45,47]. In part the exact influence will vary with the framework, but also with the way the Si/Al ratio is being controlled. Steaming is a common way to modify the Si/Al ratio post-synthetically, and the precise conditions can greatly influence the acid sites which survive. Finally, the hydrophobicity can be readily tuned by varying the Si/Al ratio, where a higher Si/Al ratio implies a more covalent species, with fewer charges due to Al substitution, making it more hydrophobic. However, increasing the Al content, resulting in a lowering of the Si/Al ratio makes the species more charged, and therefore more hydrophilic. As such the Si/Al ratio is a key parameter in designing zeolite catalysts for acid applications.

Butane isomerization has been used to test both the acidic and structural properties of solid acid catalysts, and to understand the ramifications of synthetic design and post synthetic modifications on these properties. Through the modification of Si/Al ratio in zeolites, or sulfur content in SZ, the acidity may be tuned [28,48–53]. These properties have been found to have a significant effect on the rates and derived rate constants in the mono- and bimolecular mechanisms demonstrated in butane isomerization, in conjunction with the structural aspects of the space surrounding the acid site, such as pore size and shape, which can further alter the observed selectivity through steric hinderance of the bimolecular mechanism. Due to this sensitivity, butane isomerization represents a versatile diagnostic tool for probing the effect of acid and structural changes on the synergy of the active site. For microporous zeolites, there exists a wealth of information that allows a review of what effect these individual descriptors have on butane isomerization. This in turn allows for the understanding of the

ramifications of synthetic or post-synthetic modifications on catalyst active site nature when designing novel acid catalysts.

2.2. Influence of Framework Topology

Butane isomerization has been shown to be highly responsive to active site structural descriptors within zeolite frameworks, which may alter the selectivity between the mono- and bi-molecular mechanism. ZSM-5 (MFI) and mordenite (MOR) are among the most widely studied zeolite systems for this reaction. The mordenite framework is based around small 8-membered and elliptical 12-membered channels, thus molecules may only diffuse linearly down pores, via single-file diffusion. This has been thought to hinder the bimolecular mechanism, as it hinders interactions between two molecules. In contrast cage systems such as zeolite Y (Figure 5) favor bimolecular isomerization through having larger cavities to permit the formation of the C_8 intermediate [53]. Curiously Tran et al. showed that *n*-butane isomerization is much more hindered in mordenite than *n*-hexane and *n*-heptane isomerization. This was attributed to butane proceeding by a bimolecular process, whereas the longer *n*-hexane and *n*-heptane are monomolecular processes [51]. On dealumination, the mordenite selectivity profile is altered in favor of isobutane as the mesopores improve the efficiency of diffusion, lowering the likelihood of further unwanted reactions (see also Section 2.5). Monte Carlo simulations by Kärger et al. suggest that deviating from single-file diffusion to more regular diffusion greatly increases the likelihood of reactants interacting, and thus the chances of the bimolecular pathway are improved [54]. Despite this, at lower temperatures (250 °C) mordenite, at specific Si/Al ratios has been shown to operate mainly through the bimolecular mechanism [28] under precise experimental conditions [26,55]. Though temperature was also found to play a key role, with higher temperatures (>290 °C) resulting in significant quantities of propane. Liu et al. compared mordenite with SZ and found that single file diffusion was demonstrated in pentane isomerization [56]. This was used as evidence to support the observation that the geometric constraints in mordenite inhibit isomerization under bimolecular conditions. As bimolecular isomerization requires an intermolecular interaction of a butene and butyl carbenium to form the C_8 intermediate, which is understandably hindered in single file diffusion situations [57].

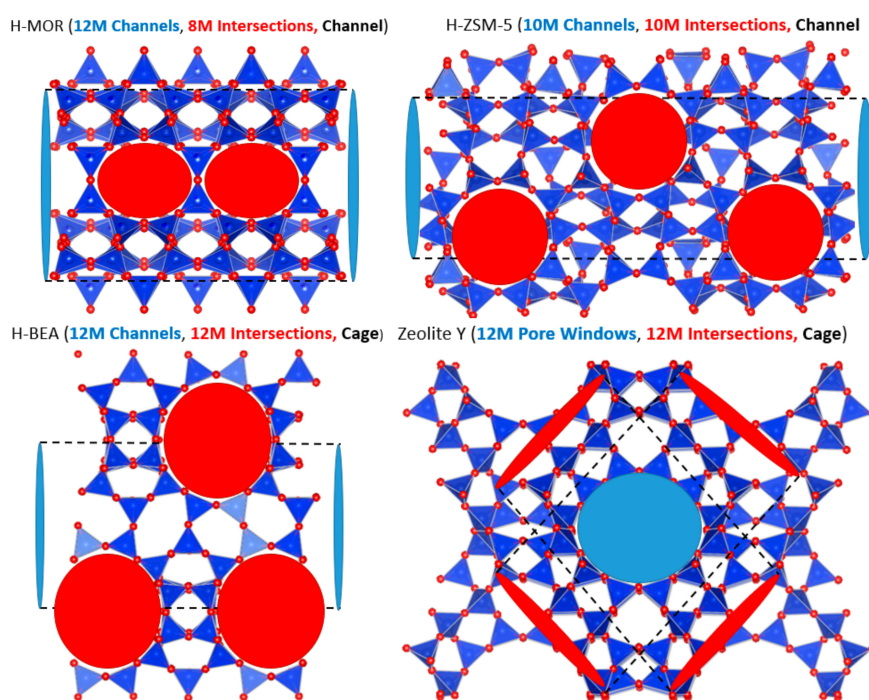


Figure 5. Schematic showing the framework topologies of a range of common zeolites investigated for butane isomerization.

Despite having a smaller 10-membered ring, systems of the ZSM-5s are also known to operate via a bimolecular pathway (Figure 5) [58]. Cañizares et al. shows that by using the bulky 1, 1, 1, 3, 3, 3-hexamethyldisilazane to poison surface BAS, the activity of mordenite-based systems was drastically affected, compared to ZSM-5 systems [26]. It was postulated that though ZSM-5 possesses a narrower pore opening (5.1–5.6 Å) than mordenite (6.5–7.0 Å), the 3-dimensional pore network of ZSM-5 aids the formation of the C₈ intermediate. This was suggested to occur at the larger channel intersections (9–10 Å wide). This is also believed to be linked to the acid site density in ZSM-5, favoring the bimolecular pathway. It was found that, unlike ZSM-5, zeolite beta can perform both the monomolecular and bimolecular pathways simultaneously, showing improved initial selectivity to isobutane. However, this lack of steric control can lead to more rapid catalyst deactivation [56]. Zeolite beta possesses a larger kinetic diameter than ZSM-5, and hence favors the formation of the bulky C₈ intermediate required by bimolecular isomerization. Yet, the narrower pores of ZSM-5 favors disproportionation products more than isomerization products, with a greater proportion of propane being formed over ZSM-5 than zeolite beta [58]. In both zeolites a C₈ intermediate can form within the pores. However, there are several different C₈ intermediates which can form, each with its own preferred cracking pathway, and associated products [59]. To achieve maximum isobutane selectivity, the C₈ intermediate would ideally break into two isobutyl products, instead of linear butyl, pentane or propane. In zeolite beta the pore is large enough to permit the pathway to yield these two isobutyl species, whereas the more confined pore geometry of ZSM-5, hinders this pathway, lowering isobutane selectivity [59].

However, it is difficult to trivialize the mechanism selectivity as the result of solely topology or acid site density, when it is often a combination of both that decides on monomolecular or bimolecular mechanism activation. Wang et al. found that ZSM-5 had a greater density of strong BAS than their zeolite beta. A previous kinetic study found that bimolecular isomerization predominated over the ZSM-5 frameworks featured in this study [60].

When comparing zeolite species, De Rossi et al. found that zeolite topology also determines stability and resistance to coking [53]. Channel structures such as mordenite and zeolite beta were found to rapidly deactivate as polyenyl unsaturated chains (coke precursors), were formed. Due to the framework topology, it only requires one such coke molecule to block an entire channel, resulting in the observed rapid deactivation in one hour. By comparison, zeolite Y (Figure 5) consisting of a multidimensional supercage, and ZSM-5 with a 2D structure, were far more resistant to coking, displaying a stable activity for over five hours [53,58]. Overall, these works show that framework topology is the key deciding factor in determining the product selectivity profile of butane isomerization. Thus, the relative contribution of the monomolecular and bimolecular mechanism can be used to gauge the spatial constraints of other acid frameworks, with similar acid site densities, for different topologies.

2.3. Influence of Acid Site Density

Studies have shown that acid site density, naturally linked to acid site concentration, is one of the key factors in determining which isomerization mechanism (monomolecular or bimolecular) is followed. Typically, monomolecular butane isomerization mechanisms require single isolated acid sites, whereas bimolecular isomerization requires adjacent sites [32,34,61,62]. This results in the rate of the bimolecular reaction being much more sensitive to the acid site density than the monomolecular rates. As a result, numerous studies have noted the reaction rates of monomolecular and bimolecular mechanisms to be first and second order respectively, in relation to acid site quantity or density. Wang et al. emphasized this by controlling the acid site density of ZSM-5 by varying the Si/Al ratio of samples from 25 to 470 [63]. By employing conditions that exclusively lead to one pathway, they were able to quantify the monomolecular and bimolecular rates of reaction, individually. In doing so they confirmed that at 350 °C, the monomolecular mechanism had an order of 0.88 with respect to the acid site density (Figure 6). In contrast the ZSM-5 under bimolecular conditions at 350 °C showed a non-linear dependency proportional with an order of 1.72, with respect to the catalytic BAS (Figure 6).

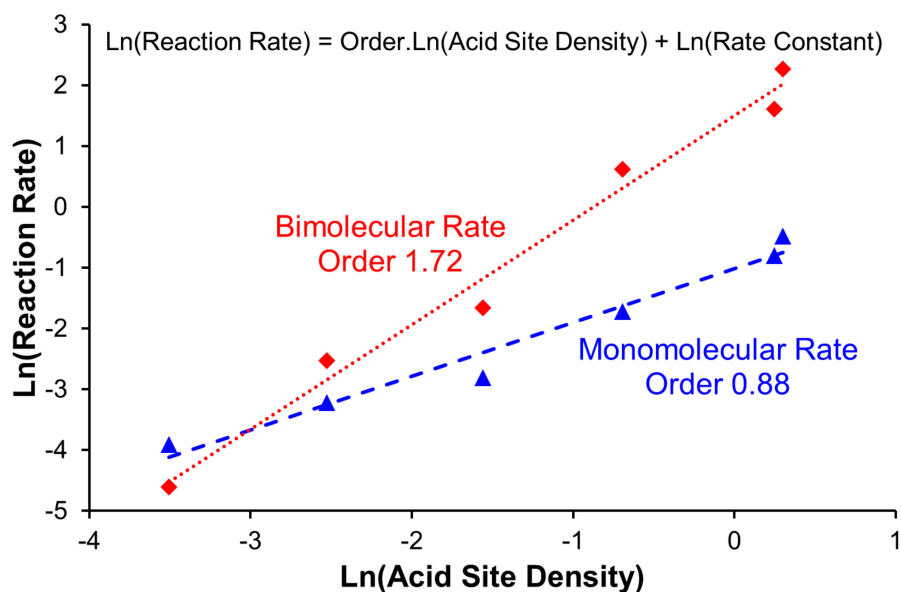


Figure 6. Analysis of the rate of reaction data for butane isomerization carried out over ZSM-5, from Wang et al. showing the varying dependence of reaction rate on acid site density, between the two mechanisms. Figure created from data in [63].

By varying Al content of mordenite through dealumination, Tran et al. explored the reaction rate of the bimolecular mechanism at 250 °C under both hydrogen and nitrogen atmospheres [52]. Under nitrogen it was suggested that the maximum activity would occur for a Si/Al ratio of between 11 and 15, which agrees with the statistical limit whereby almost all proton sites can still be isolated. Using a mordenite sample with a Si/Al of 80 showed the reaction order was close to 1 with respect to butane. This suggests that the more isolated active sites in mordenite are not able to catalyze the bimolecular pathway, and therefore promote the monomolecular mechanism instead. However, a mordenite sample with a Si/Al ratio of 10, was found to have a reaction order close to 2 with respect to *n*-butane, suggesting sufficient acid site proximity to promote the bimolecular mechanism. When the inert nitrogen atmosphere was replaced with a hydrogen atmosphere, the butane order, for the mordenite sample with a Si/Al ratio of 10, dropped from 2 to 1. This suggests that hydrogen can have a negative effect on the bimolecular mechanism, likely by decreasing the concentration of carbenium ions [52].

However, in this work Tran et al. also show that a linear relationship exists between the reaction rate and the square of the acid site density, again showing evidence for the bimolecular mechanism. Though this relationship no longer holds when the total acidity exceeds 500 $\mu\text{mol/g}$. This is because at higher aluminum content, acid sites lose strength due to poor isolation. Asuquo et al. also note that by varying the aluminum content, the maximum rate of *n*-butane conversion was obtained at a $\text{SiO}_2/\text{Al}_2\text{O}_3$ ratio of 15, with Si/Al ratios of 10 and 20 both yielding lower rates [28]. Other studies demonstrate that the maximum activity of acidic mordenite has been found at a Si/Al ratio of 15 for a variety of other target reactions [64–67]. De Rossi et al. found that ZSM-5 catalysts ranging from purely siliceous to a Si/Al ratio of 120 were catalytically inert [53]. They also found evidence where high BAS concentrations negatively affects reaction rate for ZSM-5, as previous authors had found the same relationship for mordenite (Figure 7).

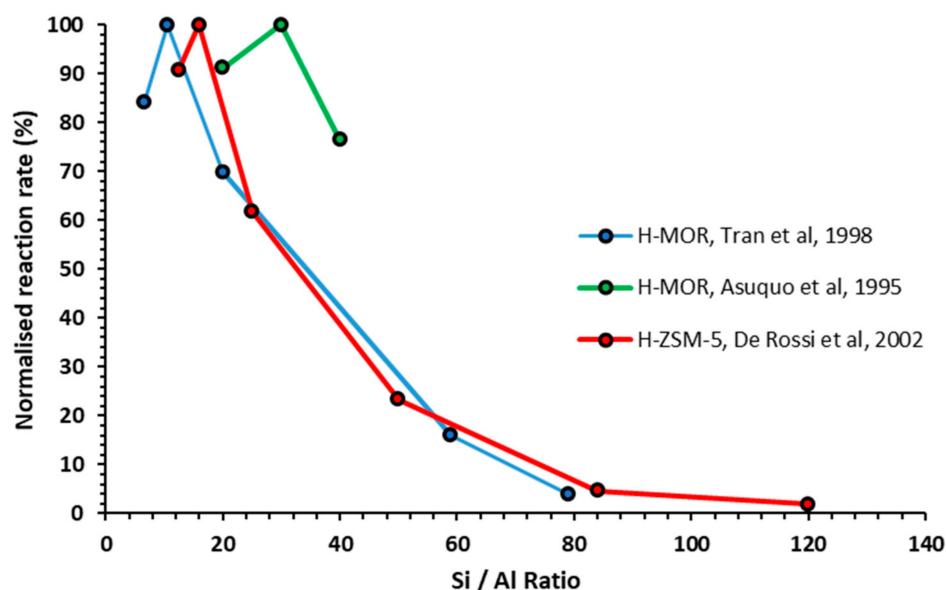


Figure 7. Correlations of butane isomerization reaction rates as a function of Si/Al ratio for different species. Rate is normalized as a percentage of maximum rate. Reaction conditions vary between data sets. Figure created using data from [28] and [51–53].

This trend between acid site quantity and rates of reaction can also be seen in conversion/selectivity relationships, as shown in a study by Kurniawan et al., investigating butane isomerization with recrystallized natural zeolites [68]. Here the quantity of BAS was found to increase with recrystallisation time. Samples with low recrystallisation times were poorly crystalline, and possessed fewer BAS. This resulted in lower *n*-butane conversion, but with a higher selectivity to isobutane, suggesting that the monomolecular mechanism was dominant. In contrast, highly crystalline samples, achieved with longer recrystallisation times, with more BAS demonstrated higher conversions with a higher selectivity to propane. This is thought to demonstrate an increasing preference for the bimolecular mechanism over the monomolecular, as acid site concentration and thus density, increased. This was also found to be the case in a ZSM-5 crystallization study by Kumar et al., where highly crystalline ZSM-5 possessed a higher quantity of BAS than poorly crystalline samples, and butane conversion scaled with acid site quantity [69].

Coking can influence the mechanism preference, especially when acid site proximity is a key factor. If, as in the monomolecular case, isolated sites are required, acid site deactivation would result in a linear decrease in conversion. However, where pairs of active sites are required, we would expect a more rapid decay in activation. For example, work by Wang et al. highlights how coking reduces the density of acidic sites causing a shift from a bimolecular to a monomolecular behavior [70]. This showed that the rate of isobutane formation did not change with coking over time, though, the selectivity to isobutane increased over time [70]. This work proposes that in the initial stages of the reaction, the super acid sites of sulfated zirconia rapidly generate butyl carbenium ions, which facilitates the bimolecular mechanism. This causes a rapid generation of coke precursors based on the high butyl carbenium ion concentration, resulting in the deactivation of acid sites, and the subsequent improvement in selectivity to isobutane as the monomolecular mechanism is increasingly favored. By using a regenerated sulfated zirconia catalyst calcined at 400 °C, a higher initial selectivity to isobutane is demonstrated than in the fresh catalyst, further supporting this argument [70]. This mechanism has been found to be applicable to other solid acid catalysts, where the acidic strength is a key factor for the rate of reaction, compared to the mechanism selectivity role that acid site concentration has been found to play.

As a result, the selectivity profile is suitable for gauging acid site density in topologically identical catalysts. Selectivity differences, when varying acid site concentrations in the same framework, may be exploited when investigating novel frameworks. For example, in aluminophosphates (the AlPO_4

analogues of zeolites), acid site density is dependent on the number of dopant sites, in a similar fashion to the Si/Al ratio of a zeolite [71]. Unlike zeolites the acid strength does not depend so much on the acid site density. This allows the influence of acid site density to be explored, independent of acid site strength, for a given system. Butane isomerization can be used to detect when the acidic property of the material reaches a maximum before acid site density begins to adversely affect reaction rates due to poor site separation. By comparing reaction profiles for frameworks with similar acid site quantities, the reaction order with respect to *n*-butane could inform investigators of how sparse or clustered the acid sites are, providing the acid strength of the materials is similar. By extending this to the myriad of dopants that are available for isomorphous substitution into aluminophosphate systems, this may serve to verify computational predictions of whether dopants substitute via an atomically clustered or distributed model [42,72,73].

2.4. Influence of Acidic Site Strength and Olefin Levels

Many studies have suggested that acidic strength is also a pivotal factor in the activity and selectivity for butane isomerization [60,61,74,75]. In order to form the butyl carbenium ion which is involved in both the monomolecular and bimolecular mechanisms, strong BAS are required. Zhang et al. demonstrate that rate of *n*-butane conversion for zeolite beta strongly depended, not on the total acidity, but specifically the quantity of strong acid sites [61].

When examining acid sites of similar strengths work by Wang et al. demonstrates that it is capable of monomolecular isomerization, even in a lower temperature range of 433–533 K [60]. By comparison, ZSM-5 structures required a higher temperature of 573–673 K in order to carry out bimolecular isomerization. By comparing the density of acid sites between samples, it was observed that the ZSM-5 (Si/Al = 38) had a higher quantity of strong BAS ($0.74 \text{ mmol}\cdot\text{g}^{-1}$), than the SZ ($0.13 \text{ mmol}\cdot\text{g}^{-1}$). On dealuminating the ZSM-5 (Si/Al = 200) a lower acidic density ($0.11 \text{ sites nm}^{-2}$) than the parent ZSM-5 (Si/Al = 38) sample ($1.39 \text{ sites nm}^{-2}$) was obtained. However, the monomolecular mechanism was not observed. This suggests that although acid site density is a crucial part in determining mechanism selectivity, the energetic barrier of the monomolecular mechanism requires a certain degree of acidic strength, where SZ demonstrates a higher acidic strength than ZSM-5.

De Rossi et al. found that acidic strength also has a role in determining the stability of materials. Here zeolite Y was found to have a lower acidic strength than WO_x/ZrO_2 [53]. Though the WO_x/ZrO_2 system had a much higher initial isobutane yield (10 mol%) than the zeolite Y (5 mol%), the zeolite Y remained stable over 5 h. In contrast the isobutane yield for the WO_x/ZrO_2 system rapidly decreased, achieving just 2 mol% isobutane yields after 3 h. This stability emphasizes how important acid strength is in forming olefinic precursors to the butyl carbenium intermediates in both monomolecular and bimolecular pathways. While olefinic species are vital species in this reaction, they are also known to have a deactivating role in isomerization [76–80]. Thus, the effect is twofold; high acidic strength promotes high concentrations of olefinic species via a high carbocation concentration, which in turn promotes a high reaction rate. As Engelhardt notes, the side reactions of cracking and disproportionation are influenced far more by the carbocation concentration than the rates of isobutane formation [79]. However high olefinic concentrations promote a high rate of coking side reactions resulting in a high deactivation rate [77,79–81]. Specifically, this is due to the selective deactivation of active sites through polyolefin coking products, preventing further carbocation formation through blockage of the active site. Larger coking products are known to also hinder diffusion through pores. Hong et al. observed with sulfated zirconia where the removal of olefins from the feed reduced the rate of deactivation, through reducing the formation rate of coke species [80]. They postulate that butene species adsorb onto active sites and oligomerize, forming typical polyolefin coke species. Chiefly, they found that strong sites were preferentially deactivated. By poisoning these strong sites with ammonia, prior to the catalytic testing, the rapid decline in activity was eliminated. Though the activity was reduced by an order of magnitude when compared with the fresh catalyst [80]. Where instead measures were taken to reduce the concentration of surface butenes present on the catalyst, a similar effect to poisoning the

strong BAS was observed. In work by Asuquo et al., the rate of catalyst deactivation was lowered by the presence of hydrogen, or water, as this reduced the olefin levels in the reaction [81]. This subsequently reduced the observed conversion rate as the bimolecular mechanism was suppressed as a result. Wulfers et al. demonstrate that by including H_2 in the reaction feed, olefinic concentrations are reduced, though reaction rate is lowered [77]. By replacing H_2 with He, reaction rates increased with olefin concentrations, although the deactivation rate likewise increased. Catalyst deactivation in mordenite was associated with butene being the precursor to coke species, where UV/Vis measurements indicated the presence of long chain polyunsaturated products thought to originate from the oligomerization of butenes.

In light of this, *n*-butane isomerization could be used as a characterization tool to measure of strong BAS in a purified *n*-butane feed. However, *n*-butane feeds commonly contain trace olefinic impurities, which can shift the rate determining step for both strong and moderate acid sites [32,34]. Olefins aid the isomerization mechanism, as they are easier to protonate than their alkane counterparts and facilitate hydride shift reactions with the more abundant butane [34,79]. Wulfers and Jentoft demonstrate that when studying mordenite activity with a purified butane feed, isomerization activity is enhanced by the addition of a miniscule 18 ppm feed of butene [76]. Further work by Wulfers et al. found that introducing butene in a time on stream experiment cause the rapid increase in the rate of isobutane rate formation, although this mainly triggered a rapid deactivation [77]. Findings from Fogash et al. supported this finding, by showing that complete removal of olefinic impurities from the feed eliminated isomerization activity in mordenite [78]. For example, Oliveira et al. note that the conversion of butane is increased when comparing sulfated and non-sulfated mordenite [74]. However, the balance of BAS and LAS is crucial for ideal isomerization. Babůrek and Nováková found that dehydroxylating zeolite samples at 650 °C under steam led to a marked decrease the number of BAS, while increasing the number of LAS [82]. The dehydroxylation process drastically decreased both the isobutane yield and selectivity compared to the parent samples [82]. This finding highlights that isomerization is more dependent on the interaction of butyl carbenium ions over BAS than LAS. As a result, the acidic strength and the dehydrogenating capabilities of catalyst are key for facilitating the formation of butyl carbenium ions, which in turn determine the rate of monomolecular or bimolecular isomerization (Figure 8).

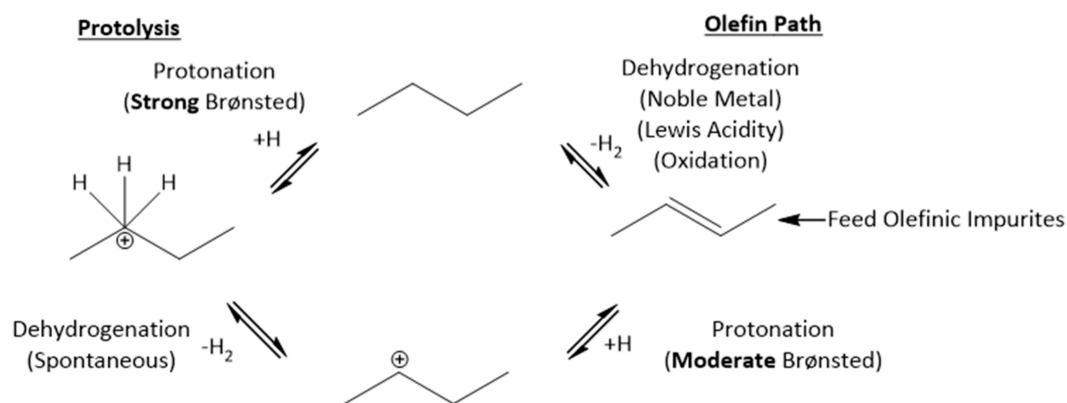


Figure 8. Influence of acid strength and dehydrogenation capability on butyl carbenium ion formation.

The observation that coking targets active sites was found to be especially pronounced on the highly acidic active sites of SZ. Wang et al. highlight how coking reduces the density of acidic sites causing a shift from a bimolecular to a monomolecular behavior [70]. Time on stream studies showed that the rate of isobutane formation did not change with coke formation over time, though the selectivity to isobutane increased. This work proposes that in the initial stages of the reaction, the super acid sites of SZ rapidly generate butyl carbenium ions, which facilitates the bimolecular mechanism [70]. This causes a rapid generation of coke precursors based on the high butyl carbenium ion concentration,

resulting in the deactivation of acid sites, and the subsequent improvement in selectivity to isobutane as the monomolecular mechanism is increasingly favored. By using a regenerated SZ catalyst calcined at 400 °C, which retained coking on active sites, a higher initial selectivity to isobutane is demonstrated than in the fresh catalyst, further supporting this argument [70]. It is thought that this behavior is applicable to the deactivation of acid site in zeolites, in addition to the physical pore blockage of large coke species.

As acidic strength is closely tied to isobutane formation and the rate of deactivation, these two parameters may provide useful indicators for assessing the behavior of other porous solid acid catalysts. As mentioned previously, aluminophosphates (AlPOs) are structurally similar to zeolites, in many cases sharing frameworks. Also, similar to zeolites, one can create acid sites within these materials by doping a range of heteroatoms into the AlPO_4 , AlPO framework. There are a wide range of divalent M^{2+} dopants one can incorporate into an AlPO to form BAS, where the specific acidic properties are a function of both the framework, and the dopant itself [43,83]. Thus, the *n*-butane consumption rate can inform investigators how effectively these active sites form butyl carbenium ions, leading to information on the reaction rate. This in turn can be used to inform investigators of relative acid strength for dopants in topologically similar materials, with similar acid site concentrations. However, this is complicated by the presence of olefins, which may occur from the feed or be generated in situ by additional functionality, such as the redox activity or Lewis acidity. Ultimately this would lead to artificially enhanced reaction rates which are not representative of acidic strength. Such functionalities are known to exist for MAIPO materials, such as the redox behavior of CoAlPOs, or the Lewis acidity of SnAlPOs [84–86].

2.5. Influence of Mesoporosity in Zeolites

When using butane isomerization as an indicator of catalyst performance it is vital to consider both the initial and longer times on stream. As sites are deactivated, this leads to the product selectivity shift from the bimolecular mechanism to the monomolecular. This could lead to misassignments of relative acid site concentration or density when comparing materials, if the product flow is not quickly analyzed. Where other framework topologies are considered as well as the role of mesoporosity on diffusion and mechanism selection, then this problem becomes more complex. Mesoporosity has been found to be crucial in determining diffusion characteristics and has been observed to improve isomerization in systems where single file diffusion is prioritized by channel topologies.

In systems which force a long residence time of products due to poor diffusion characteristics, reverse isomerization results in a high selectivity to propane. It has widely been found that by introducing mesopores in zeolites, the conversion, selectivity and lifetime has been improved, all of which has been noted in previous reviews on designing hierarchical zeolites, and their role as catalysts [87]. These effects have also been found for butane isomerization. When examining mordenite, Cañizares et al. found that the absence of mesopores in the mordenite sample studied resulted in a poor isobutane selectivity due to this [26]. In a later study, Cañizares et al. noted that the efficiency of bimolecular butane isomerization, is improved when compared to zeolites exclusively consisting of narrow channels and no mesopores [88] Tran et al. also noted that while dealuminating mordenite results in fewer acidic sites affecting selectivity, this process also introduced mesoporosity into the system. It was believed that this aided a selectivity shift to isobutane by improving diffusion characteristics, by reducing the residence time of the isobutane product in the pore system [51]. This has also been found to be the case for zeolite beta. In study by Zhang et al., it was noted that the abundant mesoporosity of the beta zeolite sample resulted in a high selectivity to isobutane when compared to non-mesoporous ZSM-5 samples, via accelerating the diffusion of feed and product molecules [58]. Oliveira et al. also note that the introduction of mesopores on the dealumination of mordenite improves accessibility to the BAS, and when combined with sulfation of the catalyst, serves to increase the initial conversion [74]. This was also noted by that steaming Y zeolites induces a mesoporosity which facilitates the diffusion of larger molecules into the zeolitic channel [89]. Christensen et al.

found a similar effect when comparing mesoporous ZSM-5 with a conventional microporous sample. Diffusion characteristics were found to be much improved for the mesoporous sample when both systems were tested via isobutane elution. Both catalysts were also tested using benzene alkylation with ethylene. The mesoporous sample demonstrated improved conversion and selectivity (18 mol % and 81 mol % respectively) compared to the microporous sample (15 mol % and 73 mol % respectively). It was thought that the introduction of mesopores improved the mass transport of molecules to and from the active site, resulting in improved conversion and selectivities [90]. Liu et al. demonstrated that the conversion and selectivity of isobutane cracking may be tuned through controlling the mesoporosity of ZSM-5 catalysts. More mesoporous samples demonstrated higher conversion and selectivities due to an improved diffusion, as well as improved catalyst stabilities and lifetimes [91]. The introduction of mesoporosity has also been found to improve resistance to coking, much like when comparing channel versus cage topologies. For *n*-hexane isomerization Modhera et al. note that desilicated ZSM-5 and zeolite beta samples feature mesoporosity which improves catalyst lifetime over the parent samples [92].

As a result, much of the diffusion problems presented by narrow pore zeolite systems can be improved by the introduction of mesopores to facilitate mass transport. Butane isomerization has been shown to be responsive to the effects of mass transport and would represent a suitable test reaction for assessing the relative effects of mesoporosity compared to microporous frameworks. When examining SZ, the combination of mesoporosity and ideal acid characteristics result in a highly active catalyst.

3. Solid-Acid Catalysts for Butane Isomerization

Besides microporous zeotypes, mesoporous catalysts of varying composition have been used or studied for butane isomerization. The majority of the literature is dedicated to SZ and zeotypes and therefore will form the focus of this discussion; however, a brief introduction to the other types of catalysts is outlined below to provide background to the field.

3.1. Friedel-Crafts Catalysts

This class of catalysts were known as the “first generation” Friedel-Crafts catalysts for hydroisomerization. This generation of catalysts includes aluminium chloride, aluminium bromide, ferric chloride, aluminium mixed with zirconium chloride, copper chloride, zinc chloride, calcium chloride, boron fluoride, and hydrogen fluoride with or without metallic nickel present, tin chloride, and zirconium chloride [93]. However, issues with the large scale commercialization of these Friedel-Crafts catalysts included high rates of corrosion, plugging of equipment and catalyst beds, as well as high catalyst consumption. In addition, butane isomerization units that utilized this class of catalyst demanded high levels of maintenance, high operating costs and showed poor efficiency on stream, thus structure-property relationships are no longer studied for these catalysts. [93,94].

3.2. Bifunctional Catalysts

Efforts to find a catalyst that could operate under low temperatures and retain conversion without the setbacks of the Friedel-Crafts catalysts led to the development of bifunctional catalysts. These were characterized by significantly enhanced acidity allowing the reduction in operating temperature without compromising conversion. These materials exhibited both hydrogenation as well as controlled-acidity components so were quickly adopted in the industry. The solid acid participates in the steps involving carbenium ions, while the metallic component offers hydrogenation-dehydrogenation activity [33].

This class of catalysts is prepared by treating alumina supported platinum with a halide compound such as, carbon tetrachloride, chloroform, methylene chloride, hexachloroethane, aluminum chloride, thionyl chloride, and sulfuryl chloride to name a few. These low temperature bifunctional hydroisomerization catalysts have the ability to operate in the same temperature regime as the Friedel-Crafts catalysts without the same limitations. [95].

3.3. Heteropoly Acids

Heteropoly acids are also an important class of isomerization catalysts, owing to their high acidity, which, akin to chlorinated alumina supports, enables isomerization at comparatively low temperatures to zeolites and SZ, an example of which is $\text{H}_3\text{PW}_{12}\text{O}_{40}$ and its associated caesium salts [96,97]. In a study carried out by Na et al. [97], they found that at 300 °C the activity and selectivity of $\text{Cs}_{2.5}\text{H}_{0.5}\text{PW}_{12}\text{O}_{40}$ were significantly higher than that of SZ which was attributed to its strong acidity and low levels of deactivation. Another study by Ono et al. [33] investigated $\text{H}_3\text{PW}_{12}\text{O}_{40}$ on and Pd/carbon support for alkane isomerization which showed higher activities at lower temperatures. This is thought to be through a similar mechanism to the Pt/SZ catalysts, where hydrogen dissociates on the metal surface to form hydrogen atoms which react with the heteropoly anion to form protons [98]. Structure property correlations from analogous noble metal doped zeolites or SZ may be used to investigate the synergistic effect of metal surfaces and acid sites in close proximity and may be applied.

3.4. Tungsten Oxide Supported on Zirconia

Another catalyst of great interest in alkane isomerization is tungsten oxide supported on zirconia, abbreviated to $\text{WO}_x\text{-ZrO}_2$ or WZ. Hino et al. reported that this type of catalyst was active for *n*-butane isomerization at operating temperatures of 50 °C [99]. They also found that the stability and selectivity to branched products was higher for Pt promoted WZ than Pt/SZ [100,101]. Other benefits of using WZ catalysts over SZ is the absence of sulfate ions which have been known to poison metal active sites [33].

3.5. Sulfated Zirconia

3.5.1. Main Principles

The limitations of both chlorinated Pt/ Al_2O_3 as well as Pt/zeolites has driven the search for a new catalyst that can meet the demands of both the market and legislation. One group of catalysts which have dominated recent research are anion modified metal oxides which exhibit adequate acidity for *n*-butane isomerization. In particular, research has focused on sulfated zirconia (SZ) which was first synthesized and used for alkane isomerization by Holm and Bailey's as describe in their 1962 patent for Phillip's Petroleum [102]. SZ possesses both Brønsted and Lewis sites, where the close arrangement of both sites serves to enhance acidity, similarly to defect sites in zeolites. This serves to set SZ apart from purely Brønsted catalysts, where the dehydrogenating ability of the Lewis sites permits a high olefin concentration, facilitating high levels of isomerization [33].

The solid-acid catalyst; SZ is created by treating amorphous zirconium oxide hydrate with sulfate solutions followed by a calcination under air at ~600 °C. Calcination of the SZ triggers a number of important processes; dehydration, crystallization and the formation of bonds between the sulfate species and the ZrO_2 surface. The resulting material is a sulfate-modified zirconia predominantly in the tetragonal phase with a small monoclinic component (Figure 9) that shows high activity in the isomerization of *n*-butane, however the synthesis of purely monoclinic SZ has been documented [103]. The nature of the crystal phase will result in the exposure of different zirconium bonding environments [104]. This inevitably effects how the zirconia interacts with sulfur species (SO_4^{2-}) during sulfation and the resulting active sites [105].

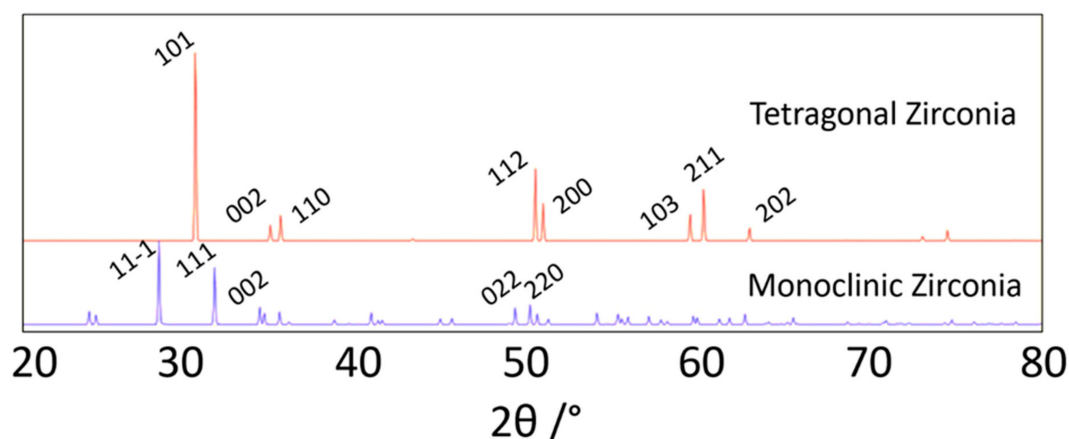


Figure 9. XRD pattern showing the different possible phases in SZ.

Typical synthetic routes for SZ catalysts produce microporous materials (pore diameter < 2 nm), with surface areas ranging from 100–120 m²/g [106], which are well suited to acid catalyzed transformations of small molecules [61]. It has been shown that the tetragonal phase of SZ is far more catalytically active than the monoclinic phase in the same reaction [107–112]. Shao et al. investigated both tetragonal and monoclinic zirconia in the preparation of solid acids SZ catalysts. They found that the phase transformation of the tetragonal ZrO₂ to monoclinic ZrO₂ occurred at calcination temperatures around 600 °C and full phase transition has occurred by 700 °C. After sulfation, the transformation from the tetragonal to monoclinic phase, even at the calcination temperature of 700 °C appeared to be inhibited by the presence of sulfur species. The tetragonal phase zirconia exhibited a more fully developed micropore structure when compared to the purely monoclinic ZrO₂. Calcination at 500 °C following sulfation produced catalysts with the highest abundance of acid active sites regardless of crystalline phase. Increasing calcination temperature enhanced the coordination of the sulfur species to the zirconia framework, although they discovered that this bonding could be damaged by the calcination temperatures in excess of 500 °C, with temperatures above 700 °C leading to pore collapse. Additionally, Shao et al. observed that sulfur and zirconium species exhibited distinctly different coordination depending on the nature of the crystalline phase. Both the BAS and LAS were observed in the tetragonal SZ catalyst, whereas mainly BAS were present in monoclinic SZ [105]. This explains the higher activity of the tetragonal phase in *n*-butane isomerization, as Song and Kydd found that the most active SZ catalyst for *n*-butane isomerization possesses around a one to one ratio of both types of acid active sites [113]. This is reinforced by Yaluris et al. [114] who have suggested that the overall activity for *n*-butane isomerization in SZ catalysts can be attributed to a dual BAS/LAS model. Several attempts have been undertaken to recreate the highly active sites in SZ using other doped zirconia species, mostly tungstated-zirconia (TZ). Though these have been shown to be far less active than SZ species at lower temperatures for alkane isomerization, as such have had considerably less attention [115]. However, studies on SZ have conclusively shown that the sulfate loading is a key metric to determine butane conversion [116].

3.5.2. Active Sites in Sulfated Zirconia

Due to the versatility of solid acid catalysts, extensive research efforts have been made to develop porous superacid materials with a high density of accessible active sites to replace molecular acid catalysts in industrial chemical transformations [117]. SZ catalysts are prevalent throughout the literature featuring *n*-butane isomerization, since first being reported by Holm and Bailey [102]. SZ was originally considered a solid “superacid”, (possessing an acidity greater than 100% H₂SO₄). However, this definition only applies to BAS, and as Olah et al. highlighted [118], the combination of BAS and LAS in SZ makes it difficult to prove beyond all doubt it is a superacid [119]. As a result, there is now a growing body of evidence that SZ does not actually exhibit “superacid” strength [107,119].

products to leave the active site to prevent unwanted by-products or reactions. It has also been shown that coking will primarily occur in the mesopores, not the micropores, preserving the microporous active sites, preventing pore blockage, thus extending their lifetime.

The dominant pathway for the isomerization of *n*-butane is thought to proceed via a bimolecular mechanism involving dimerization to form a C₈ intermediate followed by isomerization and subsequent cracking. Since this pathway involves the formation of a bulky intermediate (C₈ carbenium ion) it can be assumed that this step would be facilitated by larger pore dimensions. The size of channel openings, pore geometry and overall degree of porosity will all influence how the reaction proceeds. If the C₈ intermediate does not have adequate space to form, then the internal active metal and/or acid sites are essentially redundant [26]. Therefore, the availability of acid catalysts mesopores (2–50 nm) should be an appropriate solution to this problem. Due to the difficulties in synthesizing mesopores with a consistent pore size distribution or long range order through the top-down methods for used for mesoporous zeolites, there has been incentive for researchers to develop zirconia-based catalysts with a higher level of porosity, through the bottom-up introduction of mesopores (Figure 11) [135].

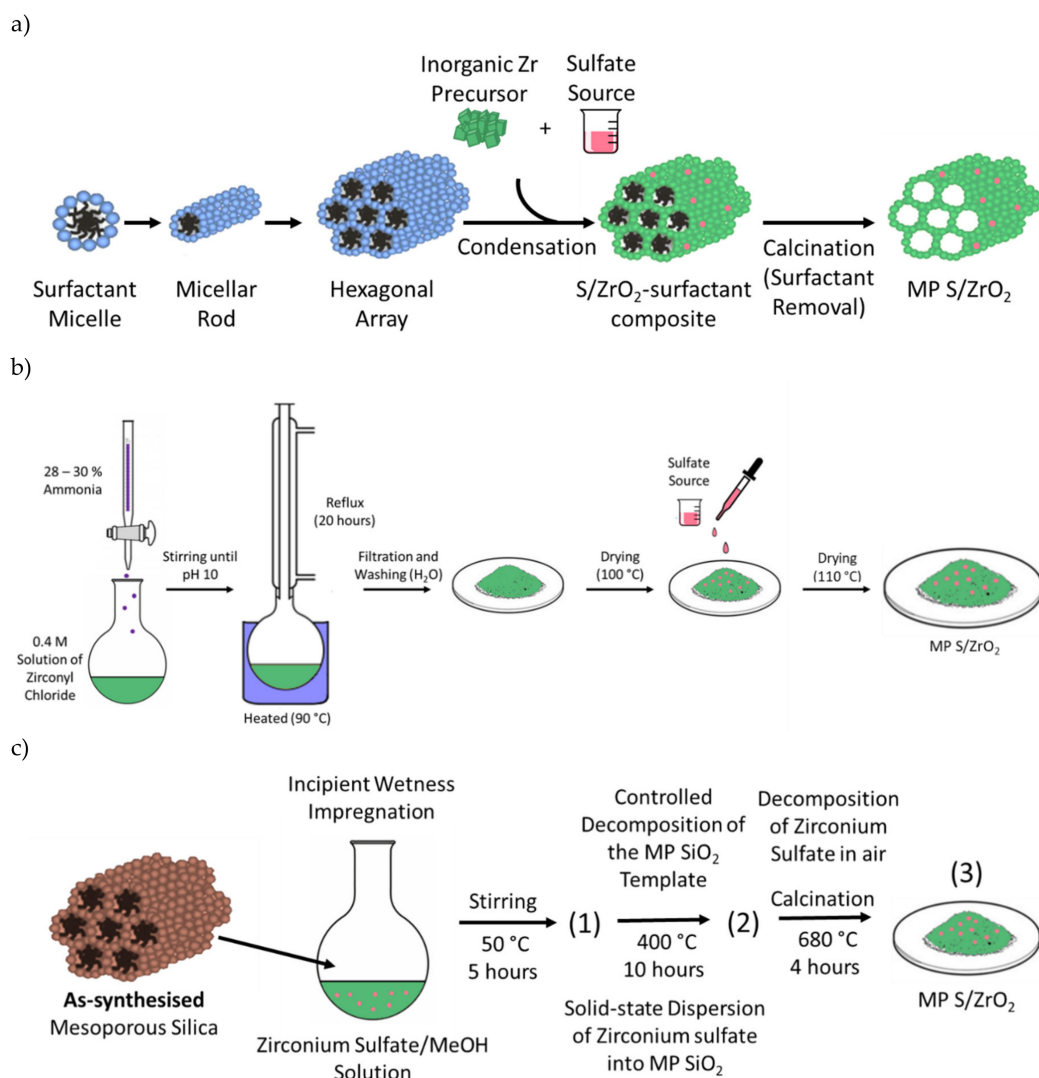


Figure 11. Schematic outlining the different ways mesopores can be introduced into SZ catalysts. (a)—Synthesis of mesoporous SZ using supramolecular assemblies of amphiphilic soft-templates as mesopore structure-directing agents; (b)—Mesoporous SZ prepared via a reflux synthetic route; (c)—Direct impregnation method for preparing SZ supported on mesoporous silica.

Inspired by Mobil researchers' M41S family of mesoporous materials [136], a range of non-siliceous oxides including TiO_2 [137], WO_3 [138], Fe_2O_3 [139] and AlPO_4 [140] have been prepared using an amphiphilic soft template (surfactants) to create mesopores during crystallization [141,142]. Similarly, there has been great interest in forming mesoporous SZ by analogous methods, due to its ability to retain a higher amount of sulfur-based active sites than other metal oxides [143–146]. Many successful attempts have created mesostructured ZrO_2 /surfactant composites, using a range of templating routes including assemblies of cationic [147–155], anionic [156–162] and neutral [135,160] amphiphiles of varying chain lengths and a number of zirconium precursors (Table 2). The addition of surfactant not only forms mesopores, but also, in most cases, increases the surface area of traditional SZ systems (typically 100–120 m^2/g). This leads to a large reactive surface, which in principle will aid the reactivity of the system.

Table 2. Comparison of different surfactants, and their effect on porosity for mesoporous zirconia-based species.

Sample	Surfactant	BET Surface Area (m^2/g)	Pore Volume (cm^3/g)	Pore Size (nm)	Ref
MP-SZ	$\text{C}_{16}\text{H}_{33}\text{N}(\text{CH}_3)_3\text{Br}$	230	0.12	2–2.5	[148]
MP-SZ	$\text{C}_{18}\text{H}_{37}\text{N}(\text{CH}_3)_3\text{Br}$	320	0.15	2–2.5	[148]
MP-SZ	$\text{C}_{20}\text{H}_{41}\text{N}(\text{CH}_3)_3\text{Br}$	390	0.22	2–2.5	[148]
MP-SZ	$\text{C}_{16}\text{H}_{33}\text{N}(\text{CH}_3)_3\text{Br}$	531	0.28	3.3	[149]
MP-SZ	$\text{C}_{16}\text{H}_{33}\text{N}(\text{CH}_3)_3\text{Br}$	373	0.17	1.8	[150]
MP-SZ	$\text{C}_{16}\text{H}_{33}\text{N}(\text{CH}_3)_3\text{Br}$	202	0.11	2.2	[163]
MP-SZ	$\text{C}_{16}\text{H}_{36}\text{NCl} + \text{acac}$	347	0.32	1.8	[135]
MP-YZ	$\text{C}_{16}\text{H}_{33}\text{N}(\text{CH}_3)_3\text{Br}$	116	0.05	1.9	[153]
MP-TiZ	$\text{C}_{16}\text{H}_{33}\text{N}(\text{CH}_3)_3\text{Br}$	423	0.19	1.8	[154]
MP-Z	$\text{C}_{16}\text{H}_{33}\text{N}(\text{CH}_3)_3\text{Br}$	269	n/A	2.8	[155]
MP-Z	$\text{C}_{12}\text{H}_{25}\text{PO}_4^{2-}$	320	N/A	2.5	[156]
MP-Z	$\text{C}_4\text{H}_9\text{PO}_4^{2-}$	233	0.21	1.5	[157]
MP-Z	$\text{C}_8\text{H}_{17}\text{PO}_4^{2-}$	313	0.23	1.9	[157]
MP-Z	$\text{C}_{12}\text{H}_{25}\text{PO}_4^{2-}$	356	0.27	2.5	[157]
MP-Z	$\text{C}_{16}\text{H}_{33}\text{PO}_4^{2-}$	361	0.33	2.6	[157]
MP-Z	$\text{C}_5\text{H}_{11}\text{COOH}$	403	N/A	1.7	[158]
MP-Z	$\text{C}_{10}\text{H}_{21}\text{COOH}$	621	N/A	3.0	[158]
MP-Z	$\text{C}_{14}\text{H}_{29}\text{SO}_4^{2-}\text{Na}^+$	N/A	N/A	N/A	[160]
MP-Z	Tergitol [®] 7	249	0.15	1.4	[160]
MP-Z	$\text{C}_{16}\text{H}_{33}\text{NH}_2$	347	0.31	1.9	[135]

One of the first challenges in synthesizing mesostructured ZrO_2 /surfactant composites is achieving a uniform array of mesopores [159,160,162]. Yet, even after the successful synthesis of a mesoporous ZrO_2 /surfactant composite, the next challenge involves removing the amphiphilic surfactant template. Typically, this is done by calcination at around 600 °C to remove the hydrocarbon-based surfactant. However mesostructured (amorphous) ZrO_2 /surfactant composites are thermally unstable, compared to a silica species, due to the differences in coordination chemistry [163,164]. Zirconium can form stable polyhedra with higher coordination numbers (6 to 8) meaning the interactions with the surfactant are stabilizing the zirconia. In contrast silicon prefers to be four coordinate, as it is in mesoporous silica, so does not bind as strongly to the surfactant. Furthermore, the inorganic ZrO_2 framework in such composites is not as well condensed as in the mesoporous silica [163,165]. As a result, removal of the surfactant template inevitably leads to pore collapse following either calcination or solvent extraction [135,148,150–152,156,166,167]. Furthermore, following the structural collapse during calcination, the zirconia species tends to crystallize and transform back into either the tetragonal or monoclinic, above temperatures of 500 °C [168]. Shao et al. showed that for amorphous ZrO_2 when calcination temperatures reach 500 °C, a phase transition to tetragonal ZrO_2 is detected [105]. With the

further increase in the calcination temperature to 600 °C, monoclinic ZrO₂ was formed from the phase transformation of tetragonal ZrO₂, but the transformation did not proceed to completion leading to a mixture of phases. With further increase in calcination temperature, the monoclinic ZrO₂ dominates as the most stable phase [105].

Fortunately, it has been found that introducing sulfate [147,148,150–152] and phosphate species [148,150–152,156,157] into ZrO₂ reinforces bonding between zirconia fragments and delays the transitions to tetragonal or monoclinic phases [105] leading to a more stable mesostructured material during template removal [159]. By tuning the sulfate concentration in the initial synthesis mixture of the zirconia/surfactant composite or employing a post-synthetic treatment, the resulting mesostructure exhibits enough thermal stability to withstand calcination to remove surfactant molecules, leaving behind modified amorphous ZrO₂ with an ordered mesoporous structure [147–152]. Thus the benefit of using sulfate species, in the synthesis of mesoporous ZrO₂, is the resulting formation of a catalytically active and thermally stable SZ with an ordered mesopore structure.

3.5.4. The Consequences of Mesoporosity on Butane Isomerization for Sulfated Zirconia Systems

Yang et al. synthesized a mesoporous (MP) SZ material [163], with hexadecyl-trimethyl-ammonium bromide (CTAB) as a surfactant template, and zirconium *n*-propoxide as the Zr precursor, in a procedure adapted from Cisela et al. [150]. Yang et al. concluded that a thermally stable MP-SZ framework could only be synthesized within a narrow range of synthetic variables: (Zr:S:CTAB) 2:2:1, calcined 540 °C in air. The activity of the successfully synthesized MP-SZ catalyst was then compared to two active microporous tetragonal SZ catalysts (MEL Cat. XZO682/01; Sulfate doped zirconium hydroxide) and Zr(SO₄)₂·4H₂O which had both been calcined [163]. During *n*-butane isomerization the single reaction product of MP-SZ was found to be isobutane. Activity of the mesoporous catalysts was also shown to be higher than the calcined Zr(SO₄)₂·4H₂O but still lower than the commercial SZ. The commercial catalyst with highest initial rate of isomerization reached a short-lived maximum in activity, before quickly deactivating. In contrast, the mesoporous sample has a much longer induction period before it reaches higher isomerization rates, but maintains conversion levels for much longer than the commercial SZ catalyst. Rather, the activity of the mesoporous sample slowly increases and reaches the same level as the commercial SZ after ~1000 min of time on stream, after the commercial catalyst has begun deactivation. In contrast the mesoporous sample showed consistent activity throughout (Figure 12) [163].

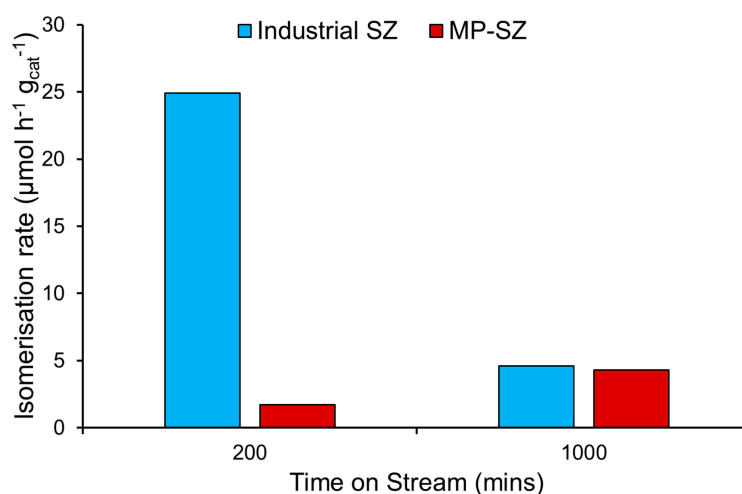


Figure 12. Catalytic data comparing MP SZ with calcined zirconia and the commercial SZ catalyst, as a function of time on stream. Replotted from data in reference 163. Reaction conditions: 200 mg of catalyst, 378 K, 1 vol % of *n*-butane in N₂, 30 mL/min-flow, atmospheric pressure.

Characterization results show that the calcined MP-SZ catalyst possesses the expected mesoporous structure with a narrow pore width distribution around 2.2 nm (Table 2) [163]. The morphology of the sample varies from the conventional SZ materials, as it is without any bulk tetragonal or monoclinic crystalline phases. Based on the reaction profiles of the commercial catalyst and the MP-SZ sample, they suggest that the high short-term activity of the commercial SZ can be attributed to highly active crystallites of bulk tetragonal zirconia, which is not present in the mesoporous sample [163].

Following on from this work, Huang et al. [135] documented their methods used to synthesize MP-SZ with crystalline pore walls of tetragonal crystal structure. They successfully synthesized MP-SZ prepared using hexadecane amine as an organic mesoporous structure-directing agent. Instead of removing the surfactant conventionally through calcination they successfully removed it via dissolution. This was followed by the material being subjected to a number of calcination programs, either as-synthesized or after deposition of sulfate groups to form SZ [135]. To do this they used acetylacetone (acac) as a stabilizing agent to slow the hydrolysis of the metal alkoxide precursors, as transition metal alkoxides are more electropositive than silicon it is important to control their hydrolysis in the presence of a surfactant template [169–171]. They found that uncontrolled hydrolysis of the zirconium propoxide precursor, even in the presence of the amine surfactant, resulted in the formation of microporous ZrO_2 [135]. Thus, they concluded both acac and an organic templating agent were needed to form a stable mesoporous tetragonal zirconia, which showed similar activity to the commercial system after 1000 min on stream (Figure 12) [135].

Risch et al. [127,172] created SZ catalysts which showed a significantly higher mesopore volume over conventional SZ synthetic methods without a surfactant via a prolonged reflux treatment modified from Knowles et al. [173,174]. The sulfur content of the commercial SZ catalyst was measured 3.24 wt %, compared to the refluxed MP-SZ which contained 4.45 wt % of sulfur [127]. The mesoporous sample had more than double the surface area of the commercial catalyst, both before sulfation and calcination. However, this increase in sulfur did not match the increase in surface area, indicating the sulfur species are likely more dispersed across the ZrO_2 surface in the MP-SZ as has been previously reported. When tested for *n*-butane isomerization they observed higher conversions with the MP-SZ catalyst, compared to the conventionally prepared SZ catalyst with a lower mesopore volume [127]. The commercial microporous SZ showed an initial activity of 30% after 5 min time on stream, which decays to 10% after 1 h. In comparison, the mesoporous catalyst displays around 20% conversion after 1 h, double that of the commercial catalyst. The isobutane selectivity of the mesoporous catalyst is comparable to that of the commercial SZ catalyst. However, higher isobutane yield values are observed from the mesoporous sample due to the improved conversion. These preliminary catalysis results show that under these reaction conditions the MP-SZ prepared via the reflux method is catalytically active for *n*-butane isomerization despite not having visible long-range order tetragonal phase crystallinity [127,172]. As discussed earlier the tetragonal crystalline phase has commonly been attributed to the activity of conventional SZ in *n*-butane isomerization [48,112]. However, the catalytic results presented in this study indicates that the MP-SZ either contains tetragonal crystallites which are too small to be seen in the X-ray diffraction, or that long-range ordered tetragonal crystallites are not required for SZ catalytic activity in *n*-butane isomerization. If the latter is true, the presence of the tetragonal phase in commercial microporous SZ catalysts could simply be a consequence of the calcination step, instead of a necessity for catalytic activity in *n*-butane isomerization.

Surface area of SZ is considered an important factor which may affect the catalytic activity, since the number of active sulfate sites is limited to the available specific surface area [175]. However as shown (Table 2) in the previous preparation methods for mesoporous zirconias, it is difficult to achieve surface areas similar to other mesoporous species by conventional preparation methods. For this reason, supporting SZ on high surface area porous materials such as SiO_2 , and Al_2O_3 was developed as an alternative to overcome these problems [109,176–178]. Lei et al. synthesized two supported SZ catalysts, $\text{SZ}/\text{Al}_2\text{O}_3$ and SZ/SiO_2 , via a standard impregnation method, comparing their activity against analogous bulk SZ [178]. As expected, the surface areas of the supported SZ samples (142–85 m^2/g

for SZ/Al₂O₃ and 280–110 m²/g for SZ/SiO₂, depending on the loading) were much higher than the unsupported SZ sample (28 m²/g), with increased SZ loading reducing the surface areas, pore volumes and pore size. Interestingly the sulfur content in the SZ/Al₂O₃ series was higher than the bulk SZ, suggesting that γ -Al₂O₃ stabilizes surface sulfur species, which was not seen for the SZ/SiO₂ samples. In low temperature (35 °C) *n*-butane isomerization SZ/Al₂O₃ increased ZrO₂ content improved catalytic activity, reaching a maximum at 60 wt % [178]. However, SZ/SiO₂ species all showed inferior activity to the bulk SZ, though activity still increased with increasing ZrO₂ content. Lei et al. suggested these trends were due to the acidity increasing on the SZ/Al₂O₃ catalysts, in comparison to a bulk SZ catalyst, which was not seen for SZ supported on SiO₂ [178]. The increased acidity of the SZ/Al₂O₃ catalysts was attributed to the tetragonal phase being stabilized by the Al₂O₃ support, thus increasing the number of strong acid sites. Though the tetragonal phase was also stabilized in the SZ/SiO₂ series, where the lower number of strong acid sites limited the catalytic activity [178]. During high temperature (250 °C) *n*-butane isomerization, as with the low temperature catalysis, both the initial and the steady activities of the SZ/Al₂O₃ catalysts increased with higher loadings of ZrO₂, up to 60% zirconia content. When compared to the bulk SZ catalyst, both initial and long-term activities of SZ/Al₂O₃ samples were greatly improved for those with zirconia loadings in the range of 30–90 wt % [178]. Although, the overall activity of each SZ/Al₂O₃ sample decreases with time on stream, as observed in the bulk SZ catalyst, the long-term activity of the SZ/Al₂O₃ samples still exceeded that of the bulk SZ catalyst after 6 h on stream. The steady activity of the 60% SZ/Al₂O₃, was shown to be 2.5 times the activity of the bulk SZ [178]. Considering the surface areas of the SZ/SiO₂ samples were improved greatly, it did not result in enhanced catalytic activity. They concluded by saying solely improving surface area does not necessarily result in the increasing catalytic activity [178].

Silica-based mesoporous materials such as MCM-41, are also potential catalyst supports because of their high thermal stability, large surface area (>1000 m²/g), uniform-sized pores and relatively small diffusion hindrance which facilitates the diffusion of molecules in and out of the mesopores. Chen et al. reported the preparation of SZ/MCM-41 via incipient wetness impregnation starting with calcined MCM-41 and zirconium sulfate [179]. Although strong acidity was observed through *n*-butane isomerization, the porous structure of MCM-41 was significantly blocked by ZrO₂ at high loadings, lowering the surface area down to 493 m²/g. They recently succeeded in synthesizing supported SZ/MCM-41 at high loadings (~60%) onto as-synthesized MCM-41 where the unremoved surfactant in the as-synthesized material served as a scaffold in stabilizing the mesostructured of SZ/MCM-41 during direct impregnation [180].

Alumina-promoted SZ was supported onto silica mesoporous silicas; MCM-41 and SBA-15 by Chen et al. via a “direct method of impregnation” followed by the solid state dispersion, removal of support template, and decomposition of the corresponding metal sulfate (Al and Zr sulfate) [179]. These mesoporous supports were able to accommodate large amounts of zirconium sulfate and stabilizing its decomposition, forming predominantly tetragonal SZ. Analysis of the textural properties showed these active phases were on the internal surface of the mesoporous materials [179]. The enhanced butane isomerization activity was attributed to the higher amount of sulfur species on the surface of these supported catalysts. Catalytic studies showed that activity was highly dependent on calcination temperature, optimal calcination temperature being 720 °C and a reaction temperature of 230 °C. Both aluminated SZ/MCM-41 and SZ/SBA-15 showed much higher catalytic activity than aluminated SZ/SiO₂ [179], likely due to the increased dispersion of the tetragonal SZ species on the mesoporous supports, stabilizing the active phase [179,180].

4. Modifying Acidity with Metal Dopants

Addition of dopant metals onto the surface of acidic porous supports has long been proven an efficient way of aiding butane isomerization, particularly when combined with a hydrogen co-feed. Although it is not a simple addition to the catalyst, there are many factors that affect the interactions of the metal with the support. A few examples being calcination/reduction conditions, metal loading

and support type, Table 3. Balancing these criteria can afford significant improvement in the catalyst activity, selectivity and stability. Primarily, studies have focussed on Pt and Pd species due to their efficacy at forming olefins.

Table 3. Catalytic systems that possess metal as nanoparticles or substituted into an acid type framework to catalyse *n*-butane isomerization.

Synthetic Variables	Deposition Method	Metal	Loading (wt %)	Support	Ref
Support and loading	Ion exchange	Pt	1.5 and 3	MOR, ZSM-5 and BEA	[181]
Support	Wetness impregnation	Pt	2	SAPO-5 and MOR	[36]
Support	Ion exchange	Pt	2	Beta and ZSM-5	[182]
Support	Incipient wetness	Pt	0.33	MOR	[76]
Support, temperature and pressure	Incipient wetness	Pt	0.5	SZ, ZSM-5, MOR and Beta	[183]
Temperature and loading	Wetness impregnation	Pt	0.02, 0.25 and 1.3	MOR	[81]
Support, Loading and metal dispersion	Wetness impregnation	Pt	0.31–0.09	FER, TON and ZSM-5	[184]
Support, loading	Impregnation	Pt	0.5, 1 and 2	MOR	[185]
Pressure and temperature	Impregnation	Pt	0.5	MOR	[186]
Metal type	Incipient wetness	Pt	0.25	SZ	[187]
Loading, deposition method and calcination conditions	Incipient Wetness/Ion exchange	Pt	0.24–0.97	ZSM-5	[188]
WHSV and carrier gas	Ion exchange	Pt	0.54	MCM-41	[38]
Support	Impregnation	Pt	0.5	SZ	[98]
Support and calcination conditions	Wetness impregnation	Pt	1.0	Carbon	[189]
Support and loading	Incipient wetness	Pd	0.27–0.57	ZSM-5 and MOR	[26]
Calcination conditions, acidity and metal precursor	Ion exchange	Pd	0.53	ZSM-5	[190]
Loading	During synthesis	Fe and Mn	2 (total)	SZ	[191]
Addition of Metal and diluent amount	Wet impregnation	La	10	ZSM-5	[192]

4.1. The Importance of Dopant-Support Combinations

The specific support chosen for metal dopants and nanoparticles is crucial in establishing synergy within the catalyst system. SZ is well recognized for catalyzing the reaction of *n*-butane isomerization due to the presence of strong BAS and LAS [49]. Early work saw addition of platinum to SZ where H₂ increased selectivity to isobutane, attributing the promoting effect to Pt addition [98]. However, it should be emphasized that it is important to combine sulfated zirconia with Pt. Pt loaded on zirconia alone results in low butane conversion, and low isobutane selectivity [193]. It has been theorized that Pt acts as de/hydrogenating agent in the formation of butenes in the *n*-butane isomerization mechanism, maintaining a butane/butene equilibrium [76,81]. This is achieved by activating hydrogen via a reverse Horiuti-Polanyi type proton transfer and carbenium ion formation by the monomolecular pathway (Figure 13) [181]. Despite this the BIC (Boreskov Institute of Catalysis) catalyst (Table 1) is a Pd/SZ species, which has higher contaminant and deactivation resilience than Pt-doped species [22]. Similarly other species have been investigated, including Al [194], Ga [194], Cr [195], Fe [195], Mn [195], Co [195], Ni [195] and Hf [196], which show some potential as promoters for SZ species.

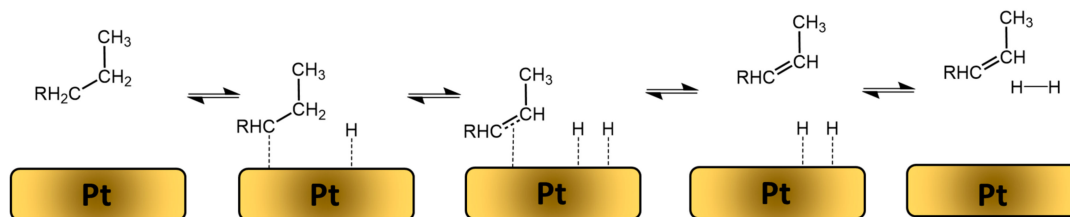


Figure 13. Suggested mechanism for the reversible butane dehydrogenation/butene hydrogenation reaction on Pt, adapted from [197].

However, whether the butane isomerization proceeds via a monomolecular or bimolecular pathway is greatly contested in the literature and is again dependent on the support type and metal loading. Out of many metals, Pt shows the greatest promoting effect in *n*-butane isomerization for dehydrogenating/hydrogenating activity [187]. In doing so Pt can balance the concentration of butane and butenes within the reaction and has a stabilizing effect on the total conversion of *n*-butane for longer time on stream (Figure 14) [36].

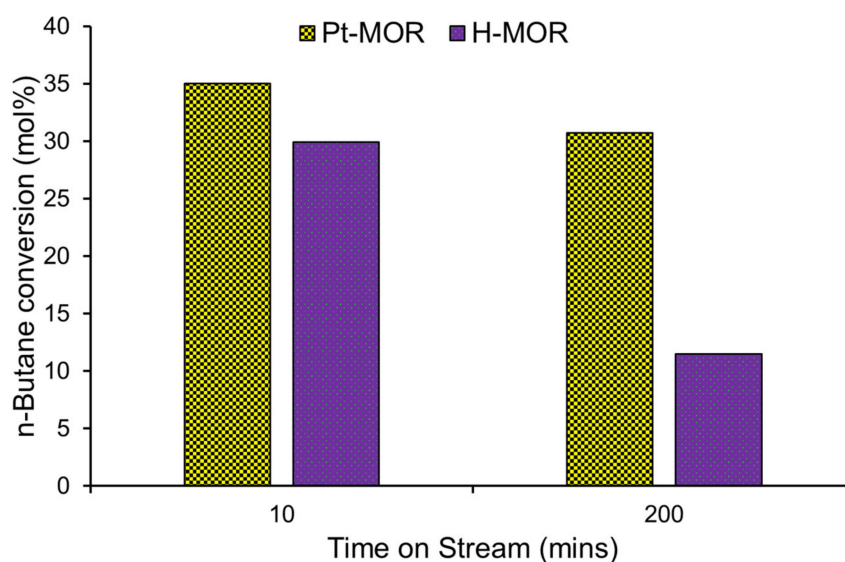


Figure 14. Showing the enhancement of Pt doping on different mordenite species for *n*-butane conversion. Figure created from data in [36]. Reaction conditions: 20% *n*-Butane and 80% hydrogen, WHSV of 3.5 hr^{−1} at 723 K.

Conversely, not all metals are a beneficial addition to the catalyst support, for example iron and manganese on SZ showed no additional benefit. For these metals a sharp increase is seen in the number of LAS but not in the number of strong BAS which are associated with the high activity in *n*-butane isomerization [191]. La on ZSM-5 also shows no significant increase in conversion, reinforcing the above findings on the reaction mechanism, alluding to the need to create the correct metal-support pairing for efficient catalysis [192].

Not all porous supports are suitable for the isomerization of *n*-butane due to their pore geometries, or acidic properties. Many supports have been evaluated to assess the effect of the acid site type and density on the catalysis of *n*-butane. One example of an inactive support for *n*-butane isomerization is MCM-41 [38]. On addition of Pt, hydrogenolysis was the main reaction observed over the catalyst, primarily showing C₁–C₄ products. It is believed the bimolecular reaction did not play a significant role due to the very small quantities of propane and pentanes formed. Instead it was proposed that the reaction proceeded by dehydrogenating *n*-butane to linear-butene, isomerization to isobutene, followed by hydrogenation to isobutane. Compared to Pt-SiO₂, Pt-MCM-41 showed greater selectivity

to isobutane (41 mol % v 11 mol %), this was attributed to the acid sites in MCM-41 being strong enough to isomerize butenes [38]. Similar observations have also been made on carbon supports [189].

Comparison of different zeolites, as discussed in Section 2, shows vast differences in butane isomerization due to pore geometry [56,126,183]. Pt-doped mordenite showed that even when there is a high dispersion of active Pt on the surface, the one-dimensional pore architecture inhibits access to acid sites located within mordenite [181]. The Pt loaded onto the surface will also cause a narrowing of the pore width, again disfavoring activity within the pores of mordenite. In contrast the pores of ZSM-5 enable the bimolecular pathway of *n*-butane isomerization despite the smaller opening to the main channel, even with the addition of Pt [181]. The three-dimensional pore system is compatible with the formation of the octyl-carbenium ions, which may account for its superior activity when compared to other undoped zeolite frameworks [26,184]. Furthermore, isobutane selectivity with Pt/ZSM-5 and Pt/MOR varied with temperature, at lower temperatures (250 °C), Pt/ZSM-5 achieved 95 mol % selectivity, whereas under identical conditions Pt/MOR achieved just 50 mol %. As the reaction temperature increased to 350 °C, the selectivity of Pt/ZSM-5 decreased to just 25 mol %, similarly Pt/MOR only achieved a 20 mol % conversion to isobutane. These species showed similar TPR and FTIR spectra, suggesting this change in selectivity must be a result of the zeolite framework [181]. The addition of platinum to mordenite shows a slight increase in isobutane selectivity compared to parent mordenite inferring there is little to no influence from Pt on the mechanistic pathways of the isomerization reaction. From FTIR analysis, it was seen that Pt binds to strong BAS and LAS within the mordenite pores due to their removal of those sites from the spectra [182,185,186]. Addition of Pt to zeolite beta and ZSM-5, while performing butane isomerization with hydrogen, increases the rate of *n*-butane isomerization compared to the parent zeolite supports. In addition, Pt and hydrogen prevent the formation of insoluble coke that leads to deactivation. This is due to the Pt sites modifying the alkane/alkene equilibrium, limiting the alkene concentration, preventing coke precursors forming [36,182].

Kumar et al. suggested that Pt addition to an acidic silicon-doped aluminophosphate (SAPO-5) significantly increased the Brønsted and Lewis acidity, possibly through some combination of the Pt species and the weaker SAPO-5 sites [36]. However, it was noted there was little effect on the total acid quantity of mordenite, but there was a drastic decrease in the number of strong acid sites, on addition of Pt to mordenite, as shown through pyridine FTIR [36]. Despite these changes both Pt/SAPO-5 and Pt/mordenite showed higher *n*-butane conversion, improved isobutane selectivity, and less influence of catalytic deactivation, compared to their parent materials [36]. Thus, the support type is important due to the pore geometry, and the existing acid sites. Both factors will influence the reaction mechanism and molecular diffusion through the framework, which is exaggerated further when metals are deposited onto the framework. The ratio of hydrogenolysis/isomerization products in this case can be indicative of catalyst design. For example, metal/support interactions and metal loading can influence product distribution, hence revealing structure property correlations.

4.2. The Influence of Dopant Loading

Generally, a better dispersion of Pt is achieved at lower loadings, thus reducing the likelihood of agglomeration of Pt particles. On zeolite beta it has been shown that a higher dispersion of Pt, increases the *n*-butane conversion [181]. In mordenite it was demonstrated that the addition of hydrogen and lower loadings of Pt would avoid the increased selectivity to hydrogenolysis which is detrimental to the isomerization mechanism. Although, a decrease in activity is sacrificed for greater stability upon the addition of Pt and hydrogen to the feed due to the lower concentration of carbocations [28]. Increasing the loading of Pt on ZSM-5 showed an increase in conversion of *n*-butane and isobutane yield due to changes in the dispersion of the Pt atoms on the surface of the framework and forces between the Pt and the zeolite [188].

The loading of the metal onto the catalyst is deemed to be sufficient when the reactions on the acid sites are rate limiting. Above this metal loading the isomerization activity has reached a maximum, and the risks increase of metal agglomeration, or having hydrogenolysis prevail [188]. Vilegas et al. reported that on adding Pt to mordenite there is a reduction in strong BAS, when heated to 723 K and pyridine absorbed in FTIR experiments, inferring Pt is bound to these strong BAS. Although the number of medium BAS increased on increasing Pt wt % (0.5–2 wt %, Figure 15), hence inferring that medium BAS were created when mordenite is impregnated with high amounts of H_2PtCl_6 . Similar behavior is observed for medium and strong LAS [185].

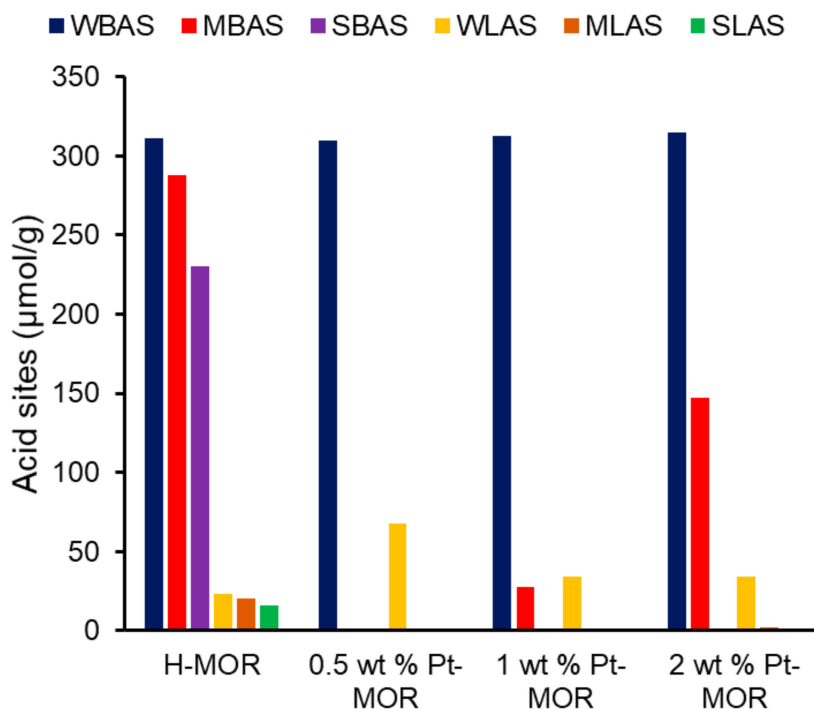


Figure 15. Showing the influence of Pt loading on acidity at different metal loadings, considering weak, medium and strong (W/M/S) Brønsted and Lewis acid sites (BAS/LAS). Adapted from data from [185].

The method by which the metal is loaded onto the catalyst has been seen to affect the activity of the catalyst. A comparison of ion exchange and impregnation methods of Pd/H-ZSM-5 shows greater selectivity when the Pd is loaded by ion exchange and when treated with a strong acid to increase acid site density [19]. The choice of dopant precursor can also influence the systems reactivity. For Pd precursors, it can be demonstrated that compared to commonly used $[\text{Pd}(\text{NH}_3)_4](\text{NO}_3)_2$, other precursors such as $\text{Pd}(\text{NO}_3)_2$ have comparable activity and better calcination procedures (Figure 16). Increasing the metal loading of Pd on ZSM-5 saw a decrease in dispersion which can be explained when all acid sites are saturated within the zeolite, excess metal will agglomerate within hidden cages within the zeolite framework, potentially causing a blockage of the pore. The drastic decrease in the surface area could affect the formation of intermediates and to an extent the access of butane to the acid site. Finally, reduction conditions can influence the dispersion of the metal on the surface of the catalyst and therefore the activity of the catalyst. The highest reduction temperature (450 °C) showed the highest isobutane yield. This is attributed to a higher dispersion of nanoparticles in hidden cages of the zeolite. Increasing the WHSV over Pt-MCM-41 shows a significant decline in the rate of conversion and higher hydrogen pressures favoring hydrogenolysis [9]. Cañizares et al. reported that reduction temperatures are influential on the dispersion of Pt atoms loaded by ion exchange whereby higher reduction temperatures reduce the activity of the catalyst also due to sintering [188,190].

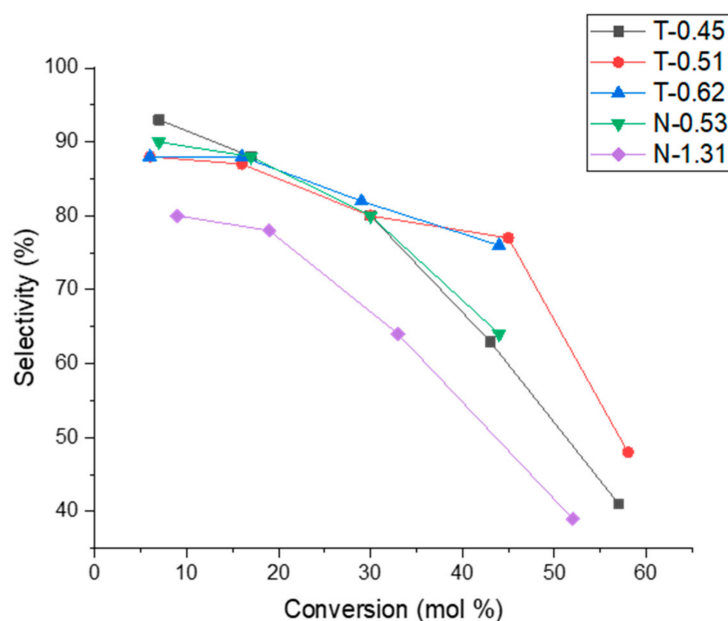


Figure 16. Effect of Pd precursor, Pd precursor; T = $[\text{Pd}(\text{NH}_3)_4](\text{NO}_3)_2$, N = $\text{Pd}(\text{NO}_3)_2$, and metal loading (0.45–1.31 wt %) on the selectivity to isobutane and conversion of *n*-butane over Pd/ZSM-5. 645 K, 1 bar, feed H_2/n -butane 10:1, figure adapted from [190].

Similar studies on sulfated zirconia alumina (SZA) catalysts by Abu et al. also investigated the influence of Pt loading on butane isomerization performance [198]. By varying the Pt loading between 0.05, 1.0 and 2.0 wt %, little influence was seen on the BET surface areas (all 110–116 m^2/g) or pore diameters (3.4–3.8 nm). However, the highest isobutane yields were achieved with 1.0 wt % Pt on SZA, again highlighting that varying the metal loading can have significant effects on selectivity. [198].

5. Conclusions

Due to the growing global demand for isobutane, the isomerization of *n*-butane is certain to play a pivotal role in the chemical industry for the foreseeable future. The topic continues to inspire researchers to continue creating novel catalysts for this specific application, with the aim of improving the conversion, selectivity, or stability of existing commercial catalysts. As this process was first commercialized in 1941, researchers approaching this field for the first time can benefit from a wealth of previous research and information on this reaction to aid their design of new catalytic materials. To this end, the various possible mechanisms are well established, with the influence of different acidic parameters well understood. This level of detail allows one to see butane isomerization, not just as an opportunity for material design, but also as a diagnostic technique for evaluating the influence of individual descriptors on catalytic activity. Many descriptors, including acid site density, type, strength and framework topology have been shown to influence this reaction.

These descriptors and their effects can be summarized as follows: acid site density influences monomolecular versus bimolecular selectivity, while the acid site strength affects reaction rate, catalyst deactivation, coking rate with the microporosity and mesoporosity inducing monomolecular/bimolecular shape-selectivity and catalyst deactivation. More importantly, the support acidity/metal balance regulates olefin availability, reactivity and coking rate, impacting monomolecular/bimolecular selectivity, and generation of secondary reactions (hydrogenolysis). As such, butane isomerization represents a versatile diagnostic tool for evaluating, optimizing and benchmarking a range of catalytic materials, in addition to the wide range of commercial applications.

Author Contributions: M.E.P. for Section 1: Commercial and Fundamental Aspects of Butane Isomerization and coordinating overall writing. J.J.M.L.B. for Section 2: Tailoring Microporous Species for Butane Isomerization. A.E.O. for Sections 2.5 and 3: Influence of Mesoporosity in Zeolites, Solid-Acid Catalysts for Butane Isomerization. E.B.M. for Section 4: Modifying Acidity with Metal Dopants. B.D.V. for commissioning research on butane isomerization, industrial sights and comparison of catalyst types. R.R. for conceiving topic of review article, planning content of review, coordinating overall content, revising text and content. All authors have read and agreed to the published version of the manuscript.

Funding: M.E.P., J.J.M.L.B., A.E.O., E.B.M. and R.R. acknowledge the Total “Consortium on Metal Nanocatalysis” project for funding. All authors have read and agreed to the submitted version of the manuscript.

Conflicts of Interest: The authors declare no conflict of interest.

References

1. LPG Production and Distribution. Available online: <https://www.wlpga.org/about-lpg/production-distribution/> (accessed on 25 June 2020).
2. Statistical Review of Global LPG. Available online: <https://www.argusmedia.com/-/media/Files/white-papers/statistical-review-of-global-lpg-2016.ashx/> (accessed on 25 June 2020).
3. Amer, M.; Wojcik, E.Z.; Sun, C.; Hoeven, R.; Hughes, J.M.X.; Faulkner, M.; Yunus, I.S.; Tait, S.; Johannissen, L.O.; Hardman, S.J.O.; et al. Low carbon strategies for sustainable bio-alkane gas production and renewable energy. *Energy Environ. Sci.* **2020**, *13*, 1818–1831. [CrossRef]
4. U.S. Energy Information Administration. *Hydrocarbon Gas Liquids (HGL): Recent Market Trends and Issues*; U.S. Department of Energy: Washington, DC, USA, 2014.
5. Singbal, S.; Yang, S.; Zhang, N. Modelling and integration of process networks for C4 hydrocarbons. *Comput. Chem. Eng.* **2020**, *140*. [CrossRef]
6. *Butane Market Size, Share & Trends Analysis Report by Application (LPG (Residential/Commercial, Chemical/Petrochemical, Industrial, Auto Fuel, Refinery), Petrochemicals, Refineries), by Region, and Segment Forecasts, 2018–2025*; Grand View Research: San Francisco, CA, USA, 2016.
7. Isobutane Market to Reach USD 34.00 Billion by 2026, Reports and Data. Available online: <https://www.globenewswire.com/news-release/2019/03/21/1758764/0/en/Isobutane-Market-To-Reach-USD-34--00-Billion-By-2026-Reports-And-Data.html> (accessed on 25 June 2020).
8. Hidalgo, J.; Zbuzek, M.; Černý, R.; Jiša, P. Current uses and trends in catalytic isomerization, alkylation and etherification processes to improve gasoline quality. *Open Chem.* **2014**, *12*, 1–13. [CrossRef]
9. Akhmadova, K.K.; Magomadova, M.K.; Syrkin, A.M.; Egutkin, N.L. History, Current State, and Prospects for Development of Isobutane Alkylation with Olefins. *Theor. Found. Chem. Eng.* **2019**, *53*, 643–655. [CrossRef]
10. Sullivan, D.; Metro, S.; Pujadó, P.R. Isomerization in Petroleum Processing. In *Handbook of Petroleum Processing*; Springer: Cham, Switzerland, 2015; pp. 479–497.
11. Echevskii, G.V.; Aksenov, D.G.; Kodenev, E.G.; Ovchinnikova, E.V.; Chumachenko, V.A. Activity of a Sulfated Zirconia Catalyst in Isomerization of n-Butane Fractions. *Pet. Chem.* **2020**, *59*, S101–S107. [CrossRef]
12. Optimising Profits by Blending Butane. Available online: <https://www.digitalrefining.com/article/1001142/optimising-profits-by-blending-butane-ti#.X2cRKYvTWUk/> (accessed on 25 June 2020).
13. You Can Just Iso My Butane: Isobutane and Isomerization in the Shale Gas World. Available online: <https://rbnenergy.com/you-can-just-iso-my-butane-isobutane-and-isomerization> (accessed on 25 June 2020).
14. Butane Isomerization. Available online: <https://www.enterpriseproducts.com/operations/petrochemical-refined-products-services/butane-isomerization> (accessed on 25 June 2020).
15. Evering, B.L. Commercial Isomerization. *Adv. Catal.* **1954**, *6*, 197–239.
16. Honeywell UOP Catalysts: Empowering Hydrocarbon Industry. Available online: <https://www.refiningandpetrochemicalsme.com/petrochemicals/24952-honeywell-uop-catalysts-empowering-hydrocarbon-industry> (accessed on 25 June 2020).
17. Klerk, A. Zeolites as Catalysts for Fuels Refining after Indirect Liquefaction Processes. *Molecules* **2018**, *23*, 115. [CrossRef]
18. Fan, D.; Tian, P.; Xu, S.; Wang, D.; Yang, Y.; Li, J.; Wang, Q.; Yang, M.; Liu, Z. SAPO-34 templated by dipropylamine and diisopropylamine: Synthesis and catalytic performance in the methanol to olefin (MTO) reaction. *New J. Chem.* **2016**, *40*, 4236–4244. [CrossRef]

19. Wang, P.; Yue, Y.; Wang, T.; Bao, X. Alkane isomerization over sulfated zirconia solid acid system. *Int. J. Energy Res.* **2020**, *44*, 3270–3294. [\[CrossRef\]](#)
20. Yan, G.X.; Wang, A.; Wachs, I.E.; Baltrusaitis, J. Critical review on the active site structure of sulfated zirconia catalysts and prospects in fuel production. *Appl. Catal. A Gen.* **2019**, *572*, 210–225. [\[CrossRef\]](#)
21. Sander, B.; Thelen, M.; Kraushaar-Czarnetzki, B. Non-corrosive and chlorine-free isomerisation process under supercritical conditions. *Catal. Today* **2002**, *75*, 119–124. [\[CrossRef\]](#)
22. Urzhuntsev, G.A.; Ovchinnikova, E.V.; Chumachenko, V.A.; Yashnik, S.A.; Zaikovskiy, V.I.; Echevsky, G.V. Isomerization of n-butane over Pd-SO₄/ZrO₂ catalyst: Prospects for commercial application. *Chem. Eng. J.* **2014**, *238*, 148–156. [\[CrossRef\]](#)
23. Bloch, H.P. *Compressors and Modern Process Applications*; John Wiley & Sons: Hoboken, NJ, USA, 2006.
24. Pines, H.; Kvetinskas, B.; Kassel, L.S.; Ipatieff, V.N. Determination of Equilibrium Constants for Butanes and Pentanes. *J. Am. Chem. Soc.* **1945**, *67*, 631–637. [\[CrossRef\]](#)
25. Surla, K.; Vleeming, H.; Guillaume, D.; Galtier, P. A single events kinetic model: N-butane isomerization. *Chem. Eng. Sci.* **2004**, *59*, 4773–4779. [\[CrossRef\]](#)
26. Cañizares, P.; de Lucas, A.; Dorado, F.; Pérez, D. Effect of zeolite pore geometry on isomerization of n-butane. *Appl. Catal. A Gen.* **2000**, *190*, 233–239. [\[CrossRef\]](#)
27. Suzuki, T.; Okuhara, T. Mechanism of Skeletal Isomerization of n-Butane Using 1,4-13C₂-n-Butane on Solid Strong Acids. *Chem. Lett.* **2000**, *29*, 470–471. [\[CrossRef\]](#)
28. Asuquo, R.A.; Edermirth, G.; Lercher, J.A. n-Butane Isomerization over Acidic Mordenite. *J. Catal.* **1995**, *155*, 376–382. [\[CrossRef\]](#)
29. Lohitharn, N.; Lotero, E.; Goodwin, J. A comprehensive mechanistic pathway for n-butane isomerization on sulfated zirconia. *J. Catal.* **2006**, *241*, 328–341. [\[CrossRef\]](#)
30. Boronat, M.; Corma, A. Are carbenium and carbonium ions reaction intermediates in zeolite-catalyzed reactions? *Appl. Catal. A Gen.* **2008**, *336*, 2–10. [\[CrossRef\]](#)
31. Boronat, M.; Viruela, P.; Corma, A. Theoretical Study on the Mechanism of the Superacid-Catalyzed Unimolecular Isomerization of n-Butane and 1-Butene. *J. Phys. Chem.* **1996**, *100*, 633–637. [\[CrossRef\]](#)
32. Caeiro, G.; Carvalho, R.H.; Wang, X.; Lemos, M.A.N.D.A.; Lemos, F.; Guisnet, M.; Ramôa Ribeiro, F. Activation of C₂–C₄ alkanes over acid and bifunctional zeolite catalysts. *J. Mol. Catal. A Chem.* **2006**, *255*, 131–158. [\[CrossRef\]](#)
33. Ono, Y. A survey of the mechanism in catalytic isomerization of alkanes. *Catal. Today* **2003**, *81*, 3–16. [\[CrossRef\]](#)
34. Guisnet, M.; Pinard, L. Characterization of acid-base catalysts through model reactions. *Catal. Rev. Sci. Eng.* **2018**, *60*, 337–436. [\[CrossRef\]](#)
35. Jain, A.V.; Pradhan, N.C.; Dalai, A.K.; Bakhshi, N.N. Studies on Chlorided Pt/Al₂O₃ Catalysts: Preparation, Characterization and n-Butane Isomerization Activity. *Catal. Lett.* **2003**, *86*, 221–227. [\[CrossRef\]](#)
36. Kumar, N.; Villegas, J.I.; Salmi, T.; Murzin, D.Y.; Heikkilä, T. Isomerization of n-butane to isobutane over Pt-SAPO-5, SAPO-5, Pt-H-mordenite and H-mordenite catalysts. *Catal. Today* **2005**, *100*, 355–361. [\[CrossRef\]](#)
37. Na, K.; Iizaki, T.; Okuhara, T.; Misono, M. Molecular design of solid acid catalysts. Isomerization of n-butane catalyzed by acid cesium salts of 12-tungstophosphoric acid combined with platinum. *J. Mol. Catal. A Chem.* **1997**, *115*, 449–455. [\[CrossRef\]](#)
38. Nieminen, V.; Kumar, N.; Salmi, T.; Murzin, D.Y. n-Butane isomerization over Pt-H-MCM-41. *Catal. Commun.* **2004**, *5*, 15–19. [\[CrossRef\]](#)
39. Del Gallo, P.; Meunier, F.; Pham-Huu, C.; Crouzet, C.; Ledoux, M.J. Selective n-Butane Isomerization over High Specific Surface Area MoO₃-Carbon-Modified Catalyst. *Ind. Eng. Chem. Res.* **1997**, *36*, 4166–4175. [\[CrossRef\]](#)
40. Yori, J.C.; Vera, C.R.; Parera, J.M. n-butane isomerization on tungsten oxide supported on zirconia. *Appl. Catal. A Gen.* **1997**, *163*, 165–175. [\[CrossRef\]](#)
41. Smith, S.; Bhattacharyya, A. Catalytic Isomerization of Butane Using Ionic Liquids. WO2014210140A1, 31 December 2014.
42. Chapman, S.; Potter, M.E.; Raja, R. The Molecular Design of Active Sites in Nanoporous Materials for Sustainable Catalysis. *Molecules* **2017**, *22*, 2127. [\[CrossRef\]](#)
43. Raja, R.; Potter, M.E.; Newland, S.H. Predictive design of engineered multifunctional solid catalysts. *Chem. Commun.* **2014**, *50*, 5940–5957. [\[CrossRef\]](#) [\[PubMed\]](#)

44. Xu, B.; Bordiga, S.; Prins, R.; van Bokhoven, J.A. Effect of framework Si/Al ratio and extra-framework aluminum on the catalytic activity of Y zeolite. *Appl. Catal. A Gen.* **2007**, *333*, 245–253. [\[CrossRef\]](#)
45. Hunger, B.; Heuchel, M.; Clark, L.A.; Snurr, R.Q. Characterization of Acidic OH Groups in Zeolites of Different Types: An Interpretation of NH₃-TPD Results in the Light of Confinement Effects. *J. Phys. Chem. B* **2002**, *106*, 3882–3889. [\[CrossRef\]](#)
46. Camiloti, A.M.; Jahn, S.L.; Velasco, N.D.; Moura, L.F.; Cardoso, D. Acidity of Beta zeolite determined by TPD of ammonia and ethylbenzene disproportionation. *Appl. Catal. A Gen.* **1999**, *182*, 107–113. [\[CrossRef\]](#)
47. Suzuki, K.; Aoyagi, Y.; Katada, N.; Choi, M.; Ryoo, R.; Niwa, M. Acidity and catalytic activity of mesoporous ZSM-5 in comparison with zeolite ZSM-5, Al-MCM-41 and silica–alumina. *Catal. Today* **2008**, *132*, 38–45. [\[CrossRef\]](#)
48. Farcasiu, D.; Li, J.Q.; Cameron, S. Preparation of sulfated zirconia catalysts with improved control of sulfur content II. Effect of sulfur content on physical properties and catalytic activity. *Appl. Catal. A Gen.* **1997**, *154*, 173–184. [\[CrossRef\]](#)
49. Chen, F.R.; Coudurier, G.; Joly, J.F.; Védrine, J.C. Superacid and Catalytic Properties of Sulfated Zirconia. *J. Catal.* **1993**, *143*, 616–626. [\[CrossRef\]](#)
50. Katada, N.; Endo, J.-I.; Notsu, K.-I.; Yasunobu, N.; Naito, N.; Niwa, M. Superacidity and Catalytic Activity of Sulfated Zirconia. *J. Phys. Chem. B* **2000**, *104*, 10321–10328. [\[CrossRef\]](#)
51. Tran, M.T.; Gnep, N.S.; Szabo, G.; Guisnet, M. Comparative study of the transformation of n-butane, n-hexane and n-heptane over H-MOR zeolites with various Si/Al ratios. *Appl. Catal. A Gen.* **1998**, *170*, 49–58. [\[CrossRef\]](#)
52. Tran, M.T.; Gnep, N.S.; Szabo, G.; Guisnet, M. Isomerization of n-Butane over H-Mordenites under Nitrogen and Hydrogen: Influence of the Acid Site Density. *J. Catal.* **1998**, *174*, 185–190. [\[CrossRef\]](#)
53. De Rossi, S.; Moretti, G.; Ferraris, G.; Gazzoli, D. Butane isomerization on several H-zeolite catalysts. In Impact of Zeolites and other Porous Materials on the new Technologies at the Beginning of the New Millennium. In Proceedings of the 2nd International FEZA (Federation of the European Zeolite Associations) Conference, Taormina, Italy, 1–5 September 2002; pp. 715–722.
54. Karger, J.; Petzold, M.; Pfeifer, H.; Ernst, S.; Weitkamp, J. Single-file diffusion and reaction in zeolites. *J. Catal.* **1992**, *136*, 283–299. [\[CrossRef\]](#)
55. Cañizares, P.; de Lucas, A.; Dorado, F. n-Butane isomerization over H-mordenite: Role of the monomolecular mechanism. *Appl. Catal. A Gen.* **2000**, *196*, 225–231. [\[CrossRef\]](#)
56. Liu, H.; Lei, G.D.; Sachtler, W.M.H. Alkane isomerization over solid acid catalysts Effects of one-dimensional micropores. *Appl. Catal. A Gen.* **1996**, *137*, 167–177. [\[CrossRef\]](#)
57. Adeeva, V.; Liu, H.Y.; Xu, B.Q.; Sachtler, W.M.H. Alkane isomerization over sulfated zirconia and other solid acids. *Top. Catal.* **1998**, *6*, 61–76. [\[CrossRef\]](#)
58. Zhang, W.; Wang, P.; Yang, C.; Li, C. A Comparative Study of n-Butane Isomerization over H-Beta and H-ZSM-5 Zeolites at Low Temperatures: Effects of Acid Properties and Pore Structures. *Catal. Lett.* **2019**, *149*, 1017–1025. [\[CrossRef\]](#)
59. Thybaut, J.W.; Marin, G.B. Multiscale Aspects in Hydrocracking: From Reaction Mechanism Over Catalysts to Kinetics and Industrial Application. *Adv. Catal.* **2016**, *59*, 109–238.
60. Wang, P.; Zhang, W.; Zhang, Q.; Xu, Z.; Yang, C.; Li, C. Comparative study of n-butane isomerization over SO₄²⁻/Al₂O₃-ZrO₂ and HZSM-5 zeolites at low reaction temperatures. *Appl. Catal. A Gen.* **2018**, *550*, 98–104. [\[CrossRef\]](#)
61. Adeeva, V.; Lei, G.D.; Sachtler, W.M.H. Competitive mechanisms of n-butane isomerization on sulfated zirconia catalysts. *Catal. Lett.* **1995**, *33*, 135–143. [\[CrossRef\]](#)
62. Adeeva, V.; Sachtler, W.M.H. Mechanism of butane isomerization over industrial isomerization catalysts. *Appl. Catal. A Gen.* **1997**, *163*, 237–243. [\[CrossRef\]](#)
63. Wang, P.Z.; Wang, S.Q.; Yue, Y.Y.; Wang, T.H.; Bao, X.J. Effects of acidity and topology of zeolites on the n-alkane conversion at low reaction temperatures. *Microporous Mesoporous Mater.* **2020**, *292*, 109748. [\[CrossRef\]](#)
64. Koradia, P. Optimization of SiO₂/Al₂O₃ mole ratio of mordenite for n-pentane isomerization. *J. Catal.* **1980**, *66*, 290–293. [\[CrossRef\]](#)
65. Guisnet, M.; Fouche, V.; Belloum, M.; Bournonville, J.P.; Travers, C. Isomerization of n-hexane on platinum dealuminated mordenite catalysts I. Influence of the silicon-to-aluminium ratio of the zeolite. *Appl. Catal.* **1991**, *71*, 283–293. [\[CrossRef\]](#)

66. Namba, S. Catalytic application of hydrophobic properties of high-silica zeolites I. Hydrolysis of ethyl acetate in aqueous solution. *J. Catal.* **1981**, *72*, 16–20. [\[CrossRef\]](#)
67. Fajula, F. Hydration of n-butenes using zeolite catalysts. Influence of the aluminium content on activity. *J. Catal.* **1984**, *89*, 60–68. [\[CrossRef\]](#)
68. Kurniawan, T.; Muraza, O.; Bakare, I.A.; Sanhoob, M.A.; Al-Amer, A.M. Isomerization of n-Butane over Cost-Effective Mordenite Catalysts Fabricated via Recrystallization of Natural Zeolites. *Ind. Eng. Chem. Res.* **2018**, *57*, 1894–1902. [\[CrossRef\]](#)
69. Kumar, N.; Nieminen, V.; Demirkan, K.; Salmi, T.; Yu Murzin, D.; Laine, E. Effect of synthesis time and mode of stirring on physico-chemical and catalytic properties of ZSM-5 zeolite catalysts. *Appl. Catal. A Gen.* **2002**, *235*, 113–123. [\[CrossRef\]](#)
70. Wang, P.; Zhang, M.; Zhang, W.; Yang, C.; Li, C. Consequence of heterogeneity of active sites for reactivity mechanism of n-butane isomerization over $\text{SO}_4^{2-}/\text{ZrO}_2\text{-Al}_2\text{O}_3$ catalyst. *Appl. Catal. A Gen.* **2017**, *542*, 311–316. [\[CrossRef\]](#)
71. Thomas, J.M.; Raja, R.; Lewis, D.W. Single-site heterogeneous catalysts. *Angew. Chem. Int. Ed. Engl.* **2005**, *44*, 6456–6482. [\[CrossRef\]](#)
72. Potter, M.E.; Paterson, A.J.; Raja, R. Transition Metal versus Heavy Metal Synergy in Selective Catalytic Oxidations. *ACS Catal.* **2012**, *2*, 2446–2451. [\[CrossRef\]](#)
73. Sastre, G.; Lewis, D.W.; Catlow, C.R.A. Modeling of silicon substitution in SAPO-5 and SAPO-34 molecular sieves. *J. Phys. Chem. B* **1997**, *101*, 5249–5262. [\[CrossRef\]](#)
74. Oliveira, A.C.; Essayem, N.; Tuel, A.; Clacens, J.-M.; Tâarit, Y.B. Comparative study of transformation of linear alkanes over modified mordenites and sulphated zirconia catalysts: Influence of the zeolite acidity on the performance of n-butane isomerization. *J. Mol. Catal. A Chem.* **2008**, *293*, 31–38. [\[CrossRef\]](#)
75. Wang, J.-H.; Mou, C.-Y. Catalytic behavior of nanostructured sulfated zirconia promoted by alumina: Butane isomerization. *Catal. Today* **2008**, *131*, 162–172. [\[CrossRef\]](#)
76. Wulfers, M.J.; Jentoft, F.C. Mechanism of n-butane skeletal isomerization on H-mordenite and Pt/H-mordenite. *J. Catal.* **2015**, *330*, 507–519. [\[CrossRef\]](#)
77. Wulfers, M.J.; Tzolova-Müller, G.; Villegas, J.I.; Murzin, D.Y.; Jentoft, F.C. Evolution of carbonaceous deposits on H-mordenite and Pt-doped H-mordenite during n-butane conversion. *J. Catal.* **2012**, *296*, 132–142. [\[CrossRef\]](#)
78. Fogash, K.B.; Hong, Z.; Kobe, J.M.; Dumesic, J.A. Deactivation of sulfated-zirconia and H-mordenite catalysts during n-butane and isobutane isomerization. *Appl. Catal. A Gen.* **1998**, *172*, 107–116. [\[CrossRef\]](#)
79. Engelhardt, J. Reaction of Butanes on Na,H-Y Zeolites and H-Mordenites. *J. Catal.* **1996**, *164*, 449–458. [\[CrossRef\]](#)
80. Hong, Z.; Fogash, K.B.; Dumesic, J.A. Reaction kinetic behavior of sulfated-zirconia catalysts for butane isomerization. *Catal. Today* **1999**, *51*, 269–288. [\[CrossRef\]](#)
81. Asuquo, R.A.; Eder-Mirth, G.; Seshan, K.; Pieterse, J.A.Z.; Lercher, J.A. Improving the Stability of H-Mordenite for n-Butane Isomerization. *J. Catal.* **1997**, *168*, 292–300. [\[CrossRef\]](#)
82. Baburek, E. Isomerization of n-butane over acid zeolites Role of Brønsted and Lewis acid sites. *Appl. Catal. A Gen.* **1999**, *185*, 123–130. [\[CrossRef\]](#)
83. Hartmann, M.; Kevan, L. Transition-metal ions in aluminophosphate and silicoaluminophosphate molecular sieves: Location, interaction with adsorbates and catalytic properties. *Chem. Rev.* **1999**, *99*, 635–664. [\[CrossRef\]](#) [\[PubMed\]](#)
84. Sankar, G.; Raja, R.; Thomas, J.M. Redox solid catalysts for the selective oxidation of cyclohexane in air. *Catal. Lett.* **1998**, *55*, 15–23. [\[CrossRef\]](#)
85. Barrett, P.A.; Sankar, G.; Catlow, C.R.A.; Thomas, J.M. X-ray Absorption Spectroscopic Study of Brønsted, Lewis, and Redox Centers in Cobalt-Substituted Aluminum Phosphate Catalysts. *J. Phys. Chem.* **1996**, *100*, 8977–8985. [\[CrossRef\]](#)
86. Mohammed, K.M.H.; Chutia, A.; Callison, J.; Wells, P.P.; Gibson, E.K.; Beale, A.M.; Catlow, C.R.A.; Raja, R. Design and control of Lewis acid sites in Sn-substituted microporous architectures. *J. Mater. Chem. A* **2016**, *4*, 5706–5712. [\[CrossRef\]](#)
87. Verboekend, D.; Pérez-Ramírez, J. Design of hierarchical zeolite catalysts by desilication. *Catal. Sci. Technol.* **2011**, *1*, 879–890. [\[CrossRef\]](#)

88. Cañizares, P.; Dorado, F.; Sánchez-Herrera, P. Hydroisomerization of n-butane over hybrid catalysts. *Appl. Catal. A Gen.* **2001**, *217*, 69–78. [\[CrossRef\]](#)
89. Stöcker, M. Gas phase catalysis by zeolites. *Microporous Mesoporous Mater.* **2005**, *82*, 257–292. [\[CrossRef\]](#)
90. Christensen, C.; Johannsen, K.; Tornqvist, E.; Schmidt, I.; Topsoe, H.; Christensen, C. Mesoporous zeolite single crystal catalysts: Diffusion and catalysis in hierarchical zeolites. *Catal. Today* **2007**, *128*, 117–122. [\[CrossRef\]](#)
91. Liu, J.; Li, Y.; Chen, Z.; Li, Z.; Yang, Q.; Hu, L.; Jiang, G.; Xu, C.; Wang, Y.; Zhao, Z. Hierarchical ZSM-5 Zeolites with Tunable Sizes of Building Blocks for Efficient Catalytic Cracking of i-Butane. *Ind. Eng. Chem. Res.* **2018**, *57*, 10327–10335. [\[CrossRef\]](#)
92. Modhera, B.K.; Chakraborty, M.; Bajaj, H.C.; Parikh, P.A. Influences of Mesoporosity Generation in ZSM-5 and Zeolite Beta on Catalytic Performance During n-Hexane Isomerization. *Catal. Lett.* **2011**, *141*, 1182–1190. [\[CrossRef\]](#)
93. McKetta, J.J.; Cunningham, W.A. *Encyclopedia of Chemical Processing and Design*; M. Dekker: New York, NY, USA, 1988.
94. Perry, S.F. Isomerization. *Ind. Eng. Chem.* **1948**, *40*, 1624–1627. [\[CrossRef\]](#)
95. McKetta, J.J., Jr. *Chemical Processing Handbook*; CRC Press: Boca Raton, FL, USA, 1993.
96. Guisnet, M. Transformation of propane, n-butane and n-hexane over $\text{H}_3\text{PW}_{12}\text{O}_{40}$ and cesium salts. Comparison to sulfated zirconia and mordenite catalysts. *Top. Catal.* **2000**, *11/12*, 247–254. [\[CrossRef\]](#)
97. Na, K.; Okuhara, T.; Misono, M. Skeletal isomerization of n-butane over caesium hydrogen salts of 12-tungstophosphoric acid. *J. Chem. Soc. Faraday Trans.* **1995**, *91*, 367–373. [\[CrossRef\]](#)
98. Ebitani, K. Skeletal isomerization of hydrocarbons over zirconium oxide promoted by Platinum and Sulfate Ion. *J. Catal.* **1991**, *130*, 257–267. [\[CrossRef\]](#)
99. Hino, M.; Arata, K. Synthesis of solid superacid of tungsten oxide supported on zirconia and its catalytic action for reactions of butane and pentane. *J. Chem. Soc. Chem. Commun.* **1988**, *18*, 1259–1260. [\[CrossRef\]](#)
100. Larsen, G.; Petkovic, L.M. Effect of preparation method and selective poisoning on the performance of platinum supported on tungstated zirconia catalysts for alkane isomerization. *Appl. Catal. A Gen.* **1996**, *148*, 155–166. [\[CrossRef\]](#)
101. Kuba, S.; Lukinskas, P.; Grasselli, R.K.; Gates, B.C.; Knözinger, H. Structure and properties of tungstated zirconia catalysts for alkane conversion. *J. Catal.* **2003**, *216*, 353–361. [\[CrossRef\]](#)
102. Holm, V.C.F.; Bailey, G.C. Sulfate-Treated Zirconia-Gel Catalyst. U.S. Patent 3032599/1962, 5 January 1962.
103. Laizet, J.B.; Söiland, A.K.; Leglise, J.; Duchet, J.C. *Top Catal.* **2000**, *10*, 89–97. [\[CrossRef\]](#)
104. Shi, G.; Yu, F.; Wang, Y.; Pan, D.; Wang, H.; Li, R. A novel one-pot synthesis of tetragonal sulfated zirconia catalyst with high activity for biodiesel production from the transesterification of soybean oil. *Renew. Energy* **2016**, *92*, 22–29. [\[CrossRef\]](#)
105. Shao, Y.; Li, Y.; Sun, K.; Zhang, Z.; Tian, H.; Gao, G.; Li, Q.; Liu, Q.; Hu, X. Sulfated Zirconia with Different Crystal Phases for the Production of Ethyl Levulinate and 5-Hydroxymethylfurfural. *Energy Technol.* **2019**, *8*. [\[CrossRef\]](#)
106. Hino, M.; Kobayashi, S.; Arata, K. Solid catalyst treated with anion. 2. Reactions of butane and isobutane catalyzed by zirconium oxide treated with sulfate ion. Solid superacid catalyst. *J. Am. Chem. Soc.* **1979**, *101*, 6439–6441. [\[CrossRef\]](#)
107. Song, X.; Sayari, A. Sulfated Zirconia-Based Strong Solid-Acid Catalysts: Recent Progress. *Catal. Rev.* **1996**, *38*, 329–412. [\[CrossRef\]](#)
108. Yamaguchi, T.; Tanabe, K.; Yao Chin, K. Preparation and characterization of ZrO_2 and SO_4^{2-} -promoted ZrO_2 . *Mater. Chem. Phys.* **1987**, *16*, 67–77. [\[CrossRef\]](#)
109. Ishida, T.; Yamaguchi, T.; Tanabe, K. Acid Property of Sulfur-Promoted Zirconium Oxide on Silica as Solid Superacid. *Chem. Lett.* **1988**, *17*, 1869–1872. [\[CrossRef\]](#)
110. Arata, K.; Hino, M. Preparation of superacids by metal oxides and their catalytic action. *Mater. Chem. Phys.* **1990**, *26*, 213–237. [\[CrossRef\]](#)
111. Arata, K. *Solid Superacids*; Academic Press: Hakodate, Japan, 1990; Volume 37, pp. 165–211.
112. Morterra, C.; Cerrato, G.; Pinna, F.; Signoreto, M. Crystal Phase, Spectral Features, and Catalytic Activity of Sulfate-Doped Zirconia Systems. *J. Catal.* **1995**, *157*, 109–123. [\[CrossRef\]](#)
113. Song, S.X.; Kydd, R.A. Activation of sulfated zirconia catalysts Effect of water content on their activity in n-butane isomerization. *J. Chem. Soc. Faraday Trans.* **1998**, *94*, 1333–1338. [\[CrossRef\]](#)

114. Yaluris, G.; Larson, R.B.; Kobe, J.M.; González, M.R.; Fogash, K.B.; Dumesic, J.A. Selective Poisoning and Deactivation of Acid Sites on Sulfated Zirconia Catalysts for n-Butane Isomerization. *J. Catal.* **1996**, *158*, 336–342. [\[CrossRef\]](#)
115. Huang, Y.-Y.; Zhao, B.-Y.; Xie, Y.-C. Modification of sulfated zirconia by tungsten oxide: Acidity enhancement and structural characterization. *Appl. Catal. A Gen.* **1998**, *171*, 75–83. [\[CrossRef\]](#)
116. Triwahyono, S.; Abdullah, Z.; Jalil, A.A. The Effect of Sulfate Ion on the Isomerization of n-Butane to iso-Butane. *J. Nat. Gas. Chem.* **2006**, *15*, 247–252. [\[CrossRef\]](#)
117. Sun, Q.; Hu, K.; Leng, K.; Yi, X.; Aguila, B.; Sun, Y.; Zheng, A.; Meng, X.; Ma, S.; Xiao, F.-S. A porous Brønsted superacid as an efficient and durable solid catalyst. *J. Mater. Chem. A* **2018**, *6*, 18712–18719. [\[CrossRef\]](#)
118. Olah, G.A.; Prakash, K.S.; Sommer, J. *Superacids*; John Wiley: New York, NY, USA, 1985. [\[CrossRef\]](#)
119. Davis, B.H.; Keogh, R.A.; Srinivasan, R. Sulfated zirconia as a hydrocarbon conversion catalyst. *Catal. Today* **1994**, *20*, 219–256. [\[CrossRef\]](#)
120. Umansky, B. On the strength of solid acids. *J. Catal.* **1991**, *127*, 128–140. [\[CrossRef\]](#)
121. Kustov, L.M.; Kazansky, V.B.; Figueras, F.; Tichit, D. Investigation of the Acidic Properties of ZrO₂ Modified by SO₂–4 Anions. *J. Catal.* **1994**, *150*, 143–149. [\[CrossRef\]](#)
122. Adeeva, V.; Dehaan, J.W.; Janchen, J.; Lei, G.D.; Schunemann, V.; Vandeven, L.J.M.; Sachtler, W.M.H.; Vansanten, R.A. Acid Sites in Sulfated and Metal-Promoted Zirconium Dioxide Catalysts. *J. Catal.* **1995**, *151*, 364–372. [\[CrossRef\]](#)
123. Babou, F.; Bigot, B.; Coudurier, G.; Sautet, P.; Védrine, J.C. 4.23 Sulfated Zirconia for n-Butane Isomerization Experimental and Theoretical Approaches. In *Acid-Base Catalysis II, Proceedings of the International Symposium on Acid-Base Catalysis II, Sapporo, Japan, 2–3 December 1993*; Elsevier Science Ltd.: Amsterdam, The Netherlands, 1994; pp. 519–529.
124. Comelli, R.A.; Vera, C.R.; Parera, J.M. Influence of ZrO₂ Crystalline Structure and Sulfate Ion Concentration on the Catalytic Activity of SO₂–4- ZrO₂. *J. Catal.* **1995**, *151*, 96–101. [\[CrossRef\]](#)
125. Liu, H.; Adeeva, V.; Lei, G.D.; Sachtler, W.M.H. Butane isomerization over platinum promoted sulfated zirconia catalysts. *J. Mol. Catal. A Chem.* **1995**, *100*, 35–48. [\[CrossRef\]](#)
126. Liu, H.; Lei, G.D.; Sachtler, W.M.H. Pentane and butane isomerization over platinum promoted sulfated zirconia catalysts. *Appl. Catal. A Gen.* **1996**, *146*, 165–180. [\[CrossRef\]](#)
127. Risch, M.; Wolf, E.E. n-Butane and n-pentane isomerization over mesoporous and conventional sulfated zirconia catalysts. *Catal. Today* **2000**, *62*, 255–268. [\[CrossRef\]](#)
128. Hino, M.; Arata, K. Synthesis of solid superacid catalyst with acid strength of H₀ ←16.04. *J. Chem. Soc. Chem. Commun.* **1980**, *18*, 851–852. [\[CrossRef\]](#)
129. Xu, B.-Q.; Sachtler, W.M.H. Isomerization of n-Butane over Deuterated Sulfated Zirconia. *J. Catal.* **1997**, *165*, 231–240. [\[CrossRef\]](#)
130. Signoretto, M.; Pinna, F.; Strukul, G.; Chies, P.; Cerrato, G.; Di Ciero, S.; Morterra, C. Platinum-Promoted and Unpromoted Sulfated Zirconia Catalysts Prepared by a One-Step Aerogel Procedure. *J. Catal.* **1997**, *167*, 522–532. [\[CrossRef\]](#)
131. Pinna, F.; Signoretto, M.; Strukul, G.; Cerrato, G.; Morterra, C. Isomerization of n-butane on sulfated zirconia: Evidence for the dominant role of Lewis acidity on the catalytic activity. *Catal. Lett.* **1994**, *26*, 339–344. [\[CrossRef\]](#)
132. Azambre, B.; Zenboury, L.; Weber, J.V.; Burg, P. Surface characterization of acidic ceria–zirconia prepared by direct sulfation. *Appl. Surf. Sci.* **2010**, *256*, 4570–4581. [\[CrossRef\]](#)
133. Na, K.; Choi, M.; Ryoo, R. Recent advances in the synthesis of hierarchically nanoporous zeolites. *Microporous Mesoporous Mater.* **2013**, *166*, 3–19. [\[CrossRef\]](#)
134. Sun, Q.; Wang, N.; Xi, D.; Yang, M.; Yu, J. Organosilane surfactant-directed synthesis of hierarchical porous SAPO-34 catalysts with excellent MTO performance. *Chem. Commun.* **2014**, *50*, 6502–6505. [\[CrossRef\]](#)
135. Huang, Y.-Y.; McCarthy, T.J.; Sachtler, W.M.H. Preparation and catalytic testing of mesoporous sulfated zirconium dioxide with partially tetragonal wall structure. *Appl. Catal. A Gen.* **1996**, *148*, 135–154. [\[CrossRef\]](#)
136. Kresge, C.T.; Vartuli, J.C.; Roth, W.J.; Leonowicz, M.E. The discovery of ExxonMobil’s M41S family of mesoporous molecular sieves. In *Mesoporous Crystals and Related Nano-Structured Materials, Proceedings of the Meeting on Mesoporous Crystals and Related Nano-Structured Materials, Stockholm, Sweden, 1–5 June 2004*; Elsevier: Amsterdam, The Netherlands, 2004; pp. 53–72.

137. Antonelli, D.M.; Ying, J.Y. Synthesis of Hexagonally Packed Mesoporous TiO₂ by a Modified Sol–Gel Method. *Angew. Chem. Int. Ed. Engl.* **1995**, *34*, 2014–2017. [\[CrossRef\]](#)
138. Huo, Q.; Margolese, D.I.; Ciesla, U.; Feng, P.; Gier, T.E.; Sieger, P.; Leon, R.; Petroff, P.M.; Schüth, F.; Stucky, G.D. Generalized synthesis of periodic surfactant/inorganic composite materials. *Nature* **1994**, *368*, 317–321. [\[CrossRef\]](#)
139. Wirnsberger, G.; Gatterer, K.; Fritzer, H.P.; Grogger, W.; Pillep, B.; Behrens, P.; Hansen, M.F.; Koch, C.B. Mesostructured Iron Oxyhydroxides. 1. Synthesis, Local Structure, and Magnetism. *Chem. Mater.* **2001**, *13*, 1453–1466. [\[CrossRef\]](#)
140. Kimura, T.; Sugahara, Y.; Kuroda, K. Synthesis of a Hexagonal Mesostructured Aluminophosphate. *Chem. Lett.* **1997**, *26*, 983–984. [\[CrossRef\]](#)
141. Monnier, A.; Schuth, F.; Huo, Q.; Kumar, D.; Margolese, D.; Maxwell, R.S.; Stucky, G.D.; Krishnamurty, M.; Petroff, P.; Firouzi, A.; et al. Cooperative formation of inorganic-organic interfaces in the synthesis of silicate mesostructures. *Science* **1993**, *261*, 1299–1303. [\[CrossRef\]](#) [\[PubMed\]](#)
142. Kresge, C.T.; Leonowicz, M.E.; Roth, W.J.; Vartuli, J.C.; Beck, J.S. Ordered mesoporous molecular sieves synthesized by a liquid-crystal template mechanism. *Nature* **1992**, *359*, 710–712. [\[CrossRef\]](#)
143. Yadav, G.D.; Murkute, A.D. Preparation of a novel catalyst UDCaT-5: Enhancement in activity of acid-treated zirconia—Effect of treatment with chlorosulfonic acid vis-à-vis sulfuric acid. *J. Catal.* **2004**, *224*, 218–223. [\[CrossRef\]](#)
144. Osatiashiani, A.; Lee, A.F.; Granollers, M.; Brown, D.R.; Olivi, L.; Morales, G.; Melero, J.A.; Wilson, K. Hydrothermally Stable, Conformal, Sulfated Zirconia Monolayer Catalysts for Glucose Conversion to 5-HMF. *ACS Catal.* **2015**, *5*, 4345–4352. [\[CrossRef\]](#)
145. Feng, Y.; Zuo, M.; Wang, T.; Jia, W.; Zhao, X.; Zeng, X.; Sun, Y.; Tang, X.; Lei, T.; Lin, L. Efficient synthesis of glucose into 5-hydroxymethylfurfural with SO₄^{2−}/ZrO₂ modified H⁺ zeolites in different solvent systems. *J. Taiwan Inst. Chem. Eng.* **2019**, *96*, 431–438. [\[CrossRef\]](#)
146. Yan, H.; Yang, Y.; Tong, D.; Xiang, X.; Hu, C. Catalytic conversion of glucose to 5-hydroxymethylfurfural over SO₄^{2−}/ZrO₂ and SO₄^{2−}/ZrO₂–Al₂O₃ solid acid catalysts. *Catal. Commun.* **2009**, *10*, 1558–1563. [\[CrossRef\]](#)
147. Sudhakar Reddy, J.; Sayari, A. Nanoporous zirconium oxide prepared using the supramolecular templating approach. *Catal. Lett.* **1996**, *38*, 219–223. [\[CrossRef\]](#)
148. Ciesla, U.; Schacht, S.; Stucky, G.D.; Unger, K.K.; Schüth, F. Formation of a Porous Zirconium Oxo Phosphate with a High Surface Area by a Surfactant-Assisted Synthesis. *Angew. Chem. Int. Ed. Engl.* **1996**, *35*, 541–543. [\[CrossRef\]](#)
149. Romannikov, V.N.; Fenelonov, V.B.; Paukshtis, E.A.; Derevyankin, A.Y.; Zaikovskii, V.I. Mesoporous basic zirconium sulfate: Structure, acidic properties and catalytic behaviour. *Microporous Mesoporous Mater.* **1998**, *21*, 411–419. [\[CrossRef\]](#)
150. Ciesla, U.; Fröba, M.; Stucky, G.; Schüth, F. Highly Ordered Porous Zirconias from Surfactant-Controlled Syntheses: Zirconium Oxide–Sulfate and Zirconium Oxo Phosphate. *Chem. Mater.* **1999**, *11*, 227–234. [\[CrossRef\]](#)
151. Schüth, F.; Ciesla, U.; Schacht, S.; Thieme, M.; Huo, Q.; Stucky, G. Ordered mesoporous silicas and zirconias: Control on length scales between nanometer and micrometer. *Mater. Res. Bull.* **1999**, *34*, 483–494. [\[CrossRef\]](#)
152. Lindén, M.; Blanchard, J.; Schacht, S.; Schunk, S.A.; Schüth, F. Phase Behavior and Wall Formation in Zr(SO₄)₂/CTABr and TiOSO₄/CTABr Mesophases. *Chem. Mater.* **1999**, *11*, 3002–3008. [\[CrossRef\]](#)
153. Mamak, M.; Coombs, N.; Ozin, G. Mesoporous Yttria-Zirconia and Metal-Yttria-Zirconia Solid Solutions for Fuel Cells. *Adv. Mater.* **2000**, *12*, 198–202. [\[CrossRef\]](#)
154. Chen, H.-R.; Shi, J.-L.; Yu, J.; Wang, L.-Z.; Yan, D.-S. Synthesis of titanium-doped ordered porous zirconium oxide with high-surface-area. *Microporous Mesoporous Mater.* **2000**, *39*, 171–176. [\[CrossRef\]](#)
155. Pârvulescu, V.I.; Pârvulescu, V.; Endruschat, U.; Lehmann, C.W.; Grange, P.; Poncelet, G.; Bönnemann, H. Preparation and characterization of mesoporous zirconium oxide. Part 2. *Microporous Mesoporous Mater.* **2001**, *44–45*, 221–226.
156. Wong, M.S.; Antonelli, D.M.; Ying, J.Y. Synthesis and characterization of phosphated mesoporous zirconium oxide. *Nanostructured Mater.* **1997**, *9*, 165–168. [\[CrossRef\]](#)
157. Wong, M.S.; Ying, J.Y. Amphiphilic Templating of Mesostructured Zirconium Oxide. *Chem. Mater.* **1998**, *10*, 2067–2077. [\[CrossRef\]](#)

158. Antonelli, D.M. Synthesis and Mechanistic Studies of Sulfated Meso- and Microporous Zirconias with Chelating Carboxylate Surfactants. *Adv. Mater.* **1999**, *11*, 487–492. [\[CrossRef\]](#)
159. Huang, Y.; Sachtler, W.M.H. Preparation of mesostructured lamellar zirconia. *Chem. Commun.* **1997**, *13*, 1181–1182. [\[CrossRef\]](#)
160. Pacheco, G.; Zhao, E.; Diaz Valdes, E.; Garcia, A.; Fripiat, J.J. Microporous zirconia from anionic and neutral surfactants. *Microporous Mesoporous Mater.* **1999**, *32*, 175–188. [\[CrossRef\]](#)
161. Zhao, E.; Hardcastle, S.E.; Pacheco, G.; Garcia, A.; Blumenfeld, A.L.; Fripiat, J.J. Aluminum-doped mesoporous zirconia obtained from anionic surfactants. *Microporous Mesoporous Mater.* **1999**, *31*, 9–21. [\[CrossRef\]](#)
162. Pacheco, G.; Fripiat, J.J. Physical Chemistry of the Thermal Transformation of Mesoporous and Microporous Zirconia. *J. Phys. Chem. B* **2000**, *104*, 11906–11911. [\[CrossRef\]](#)
163. Yang, X.; Jentoft, F.C.; Jentoft, R.E.; Girgsdies, F.; Ressler, T. Sulfated zirconia with ordered mesopores as an active catalyst for n-butane isomerization. *Catal. Lett.* **2002**, *81*, 25–31. [\[CrossRef\]](#)
164. Wang, Z.; Xu, Q.; Xu, M.; Wang, S.; You, J. In situ spectroscopic studies of decomposition of ZrSiO₄ during alkali fusion process using various hydroxides. *Rsc. Adv.* **2015**, *5*, 11658–11666. [\[CrossRef\]](#)
165. Stein, A.; Fendorf, M.; Jarvie, T.P.; Mueller, K.T.; Benesi, A.J.; Mallouk, T. E Salt-Gel Synthesis of Porous Transition-Metal Oxides. *Chem. Mater.* **1995**, *7*, 304–313. [\[CrossRef\]](#)
166. Schüth, F. Surface Properties and Catalytic Performance of Novel Mesostructured Oxides. *Ber. Der. Bunsenges. Phys. Chem.* **1995**, *99*, 1306–1315. [\[CrossRef\]](#)
167. Larsen, G.; Lotero, E.; Nabity, M.; Petkovic, L.M.; Shobe, D.S. Surfactant-Assisted Synthesis of Mesoporous Zirconia Powders with High Surface Areas. *J. Catal.* **1996**, *164*, 246–248. [\[CrossRef\]](#)
168. Simha, N.K. Crystallography of the Tetragonal → Monoclinic Transformation in Zirconia. *J. Phys. Iv.* **2014**, *5*, C8-1121–C8-1126. [\[CrossRef\]](#)
169. Livage, J.; Henry, M.; Sanchez, C. Sol-gel chemistry of transition metal oxides. *Prog. Solid State Chem.* **1988**, *18*, 259–341. [\[CrossRef\]](#)
170. Debsikdar, J.C. Transparent zirconia gel-monolith from zirconium alkoxide. *J. Non-Cryst. Solids* **1986**, *86*, 231–240. [\[CrossRef\]](#)
171. Sanchez, C.; Livage, J.; Henry, M.; Babonneau, F. Chemical modification of alkoxide precursors. *J. Non-Cryst. Solids* **1988**, *100*, 65–76. [\[CrossRef\]](#)
172. Risch, M.; Wolf, E.E. Effect of the preparation of a mesoporous sulfated zirconia catalyst in n-butane isomerization activity. *Appl. Catal. A Gen.* **2001**, *206*, 283–293. [\[CrossRef\]](#)
173. Knowles, J.A.; Hudson, M.J. Preparation and characterisation of mesoporous, high surface area zirconium(IV) oxides. *J. Chem. Soc. Chem. Commun.* **1995**, *20*, 2083–2084. [\[CrossRef\]](#)
174. Hudson, M.J.; Knowles, J.A. Preparation and characterisation of mesoporous, high-surface-area zirconium(IV) oxide. *J. Mater. Chem.* **1996**, *6*, 89–95. [\[CrossRef\]](#)
175. Corma, A.; Fornés, V.; Juan-Rajadell, M.I.; Nieto, J.M.L. Influence of preparation conditions on the structure and catalytic properties of SO₄^{2−}/ZrO₂ superacid catalysts. *Appl. Catal. A Gen.* **1994**, *116*, 151–163. [\[CrossRef\]](#)
176. Grau, J.M.; Vera, C.R.; Parera, J.M. Alternatives for a better performance of Pt in SO₄^{2−}-ZrO₂ catalysts for n-octane hydroisomerization-cracking. Selective adsorption of Pt over composites of SO₄^{2−}-ZrO₂ mixed or supported onto Al₂O₃ and SiO₂. *Appl. Catal. A Gen.* **1998**, *172*, 311–326. [\[CrossRef\]](#)
177. Huang, Y.-Y.; Zhao, B.-Y.; Xie, Y.-C. A new method to prepare silica- or alumina-supported sulfated zirconia. *Appl. Catal. A Gen.* **1998**, *173*, 27–35. [\[CrossRef\]](#)
178. Lei, T.; Xu, J.S.; Tang, Y.; Hua, W.M.; Gao, Z. New solid superacid catalysts for n-butane isomerization: γ-Al₂O₃ or SiO₂ supported sulfated zirconia. *Appl. Catal. A Gen.* **2000**, *192*, 181–188. [\[CrossRef\]](#)
179. Chen, C.-L.; Li, T.; Cheng, S.; Xu, N.; Mou, C.-Y. Catalytic Behavior of Alumina-Promoted Sulfated Zirconia Supported on Mesoporous Silica in Butane Isomerization. *Catal. Lett.* **2002**, *78*, 223–229. [\[CrossRef\]](#)
180. Chen, C.-L.; Li, T.; Cheng, S.; Lin, H.-P.; Bhongale, C.J.; Mou, C.-Y. Direct impregnation method for preparing sulfated zirconia supported on mesoporous silica. *Microporous Mesoporous Mater.* **2001**, *50*, 201–208. [\[CrossRef\]](#)
181. Baburek, E.; Nováková, J. Effect of platinum in bifunctional isomerization of n-butane over acid zeolites. *Appl. Catal. A Gen.* **2000**, *190*, 241–251. [\[CrossRef\]](#)
182. Villegas, J.; Kumar, N.; Heikkilä, T.; Lehto, V.; Salmi, T.; Murzin, D. Isomerization of n-butane to isobutane over Pt-modified Beta and ZSM-5 zeolite catalysts: Catalyst deactivation and regeneration. *Chem. Eng. J.* **2006**, *120*, 83–89. [\[CrossRef\]](#)

183. Chao, K.J.; Wu, H.C.; Leu, L.J. Skeletal Isomerization of n-Butane on Zeolites and Sulfated Zirconium Oxide Promoted by Platinum: Effect of Reaction Pressure. *J. Catal.* **1995**, *157*, 289–293. [[CrossRef](#)]
184. Pirngruber, G.D.; Zinck-Stagno, O.P.E.; Seshan, K.; Lercher, J.A. The Effect of the Pore Structure of Medium-Pore Zeolites on the Dehydroisomerization of n-Butane: A Comparison of Pt-FER, Pt-TON, and Pt-ZSM5. *J. Catal.* **2000**, *190*, 374–386. [[CrossRef](#)]
185. Villegas, J.I.; Kumar, N.; Salmi, T.; Murzin, D.Y.; Heikkilä, T.; Hudec, P.; Smiešková, A. Isomerization of n-butane over Pt-modified mordenite zeolite catalysts: Effect of Pt loadings and dealumination. In *Molecular Sieves: From Basic Research to Industrial Applications, Proceedings of the 3rd International Zeolite Symposium (3rd FEZA), Prague, Czech Republic, 23–26 August 2005*; Elsevier: Amsterdam, The Netherlands, 2005; pp. 1859–1866.
186. Nieminen, V.; Kangas, M.; Salmi, T.; Murzin, D.Y. Kinetic Study of n-Butane Isomerization over Pt-H-Mordenite. *Ind. Eng. Chem. Res.* **2005**, *44*, 471–484. [[CrossRef](#)]
187. Yori, J.C.; Parera, J.M. n-Butane isomerization on metal-promoted sulfated zirconia. *Appl. Catal. A Gen.* **1996**, *147*, 145–157. [[CrossRef](#)]
188. Cañizares, P.; De Lucas, A.; Valverde, J.L.; Dorado, F. n-Butane Hydroisomerization over Pt/HZSM-5 Catalysts. *Ind. Eng. Chem. Res.* **1997**, *36*, 4797–4808. [[CrossRef](#)]
189. Moreno-Castilla, C.; Porcel-Jiménez, A.; Carrasco-Marín, F.; Utrera-Hidalgo, E. Pt/carbon catalysts: Effect of pretreatment on the dispersion and morphology of the Pt particles, on their capacity to chemisorb H₂ and on the H₂/n-C₄H₁₀ reaction. *J. Mol. Catal.* **1991**, *66*, 329–341. [[CrossRef](#)]
190. Cañizares, P.; de Lucas, A.; Dorado, F.; Aguirre, J. n-Butane hydroisomerization over Pd/HZSM-5 catalysts. Palladium loaded by ion exchange. *Microporous Mesoporous Mater.* **2001**, *42*, 245–254. [[CrossRef](#)]
191. Løften, T.; Gnep, N.S.; Guisnet, M.; Blekkan, E.A. Iron and manganese promoted sulfated zirconia: Acidic properties and n-butane isomerization activity. *Catal. Today* **2005**, *100*, 397–401. [[CrossRef](#)]
192. Rahimi, N.; Karimzadeh, R. Kinetic modeling of catalytic cracking of C₄ alkanes over La/HZSM-5 catalysts in light olefin production. *J. Anal. Appl. Pyrolysis* **2015**, *115*, 242–254. [[CrossRef](#)]
193. Grau, J. Crystal phase dependent metal-support interactions in Pt/SO₄–ZrO₂ catalysts for hydroconversion of n-alkanes. *Appl. Catal. A Gen.* **2004**, *265*, 141–152. [[CrossRef](#)]
194. Hwang, C.-C.; Mou, C.-Y. Comparison of the promotion effects on sulfated mesoporous zirconia catalysts achieved by alumina and gallium. *Appl. Catal. A Gen.* **2009**, *365*, 173–179. [[CrossRef](#)]
195. McIntosh, D.J.; Kydd, R.A.; Hill, J.M. Comparison of Cr, Mn, Fe, Co, and Ni as promoters for n-Butane conversion over sulfated zirconia. *Chem. Eng. Commun.* **2004**, *191*, 137–149. [[CrossRef](#)]
196. Ahmed, M.A. Surface characterization and catalytic activity of sulfated-hafnia promoted zirconia catalysts for n-butane isomerization. *Fuel Process. Technol.* **2011**, *92*, 1121–1128. [[CrossRef](#)]
197. Sattler, J.J.; Ruiz-Martinez, J.; Santillan-Jimenez, E.; Weckhuysen, B.M. Catalytic dehydrogenation of light alkanes on metals and metal oxides. *Chem Rev.* **2014**, *114*, 10613–10653. [[CrossRef](#)]
198. Abu, I.I.; Das, D.D.; Mishra, H.K.; Dalai, A.K. Studies on platinum-promoted sulfated zirconia alumina: Effects of pretreatment environment and carrier gas on n-butane isomerization and benzene alkylation activities. *J. Colloid Interface Sci.* **2003**, *267*, 382–390. [[CrossRef](#)]

